RIGA TECHNICAL UNIVERSITY

Abhishek Rajesh Indurkar

AMORPHOUS CALCIUM PHOSPHATES AND THEIR NANOCOMPOSITES

Summary of the Doctoral Thesis

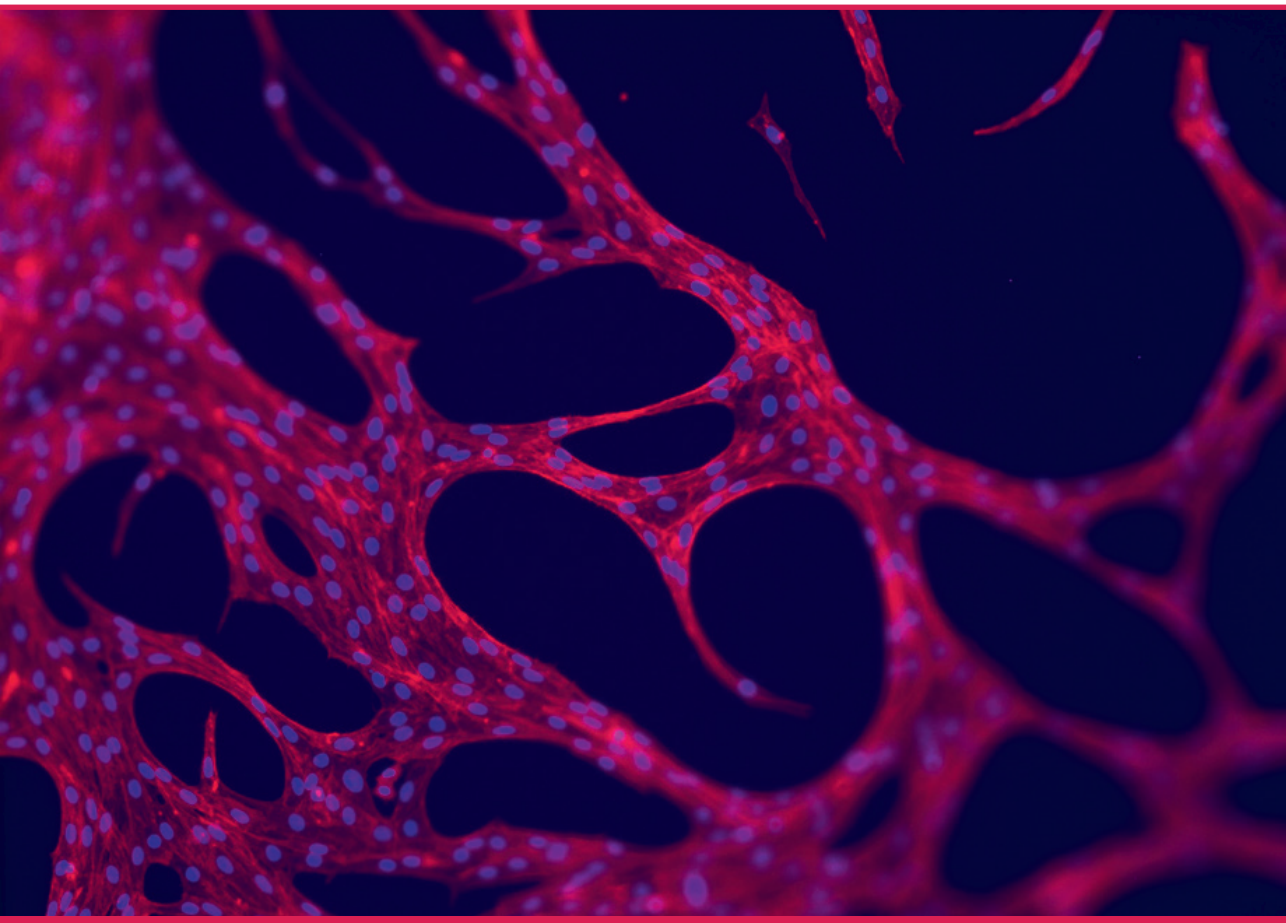

RTU Press
Riga 2024

RIGA TECHNICAL UNIVERSITY
Faculty of Natural Sciences and Technology
Institute of Biomaterials and Bioengineering

Abhishek Rajesh Indurkar
Doctoral Student of the Study Programme "Chemistry, Materials Science and Engineering"

AMORPHOUS CALCIUM PHOSPHATES AND THEIR NANOCOMPOSITES

Summary of the Doctoral Thesis

Scientific supervisor
Professor Dr. sc. ing. JĀNIS LOČS

Co-supervisor
Dr. sc. ing. KRISTAPS RUBENIS

RTU Press
Riga 2024

Indurkar, A. R. Amorphous Calcium Phosphates and Their Nanocomposites. Summary of the Doctoral Thesis. Riga: RTU Press, 2024. 39 p.

Published in accordance with the decision of the Promotion Council "P-02" of 28th August 2024,
Minutes No. 04030-9.2.2/6.

Cover picture by Abhishek Rajesh Indurkar

https://doi.org/10.7250/9789934371028
ISBN 978-9934-37-102-8 (pdf)

DOCTORAL THESIS PROPOSED TO RIGA TECHNICAL UNIVERSITY FOR PROMOTION TO THE SCIENTIFIC DEGREE OF DOCTOR OF SCIENCE

To be granted the scientific degree of Doctor of Science (Ph. D.), the present Doctoral Thesis has been submitted for defence at the open meeting of the RTU Promotion Council on 28th August 2024 at the Faculty of Natural Sciences and Technology of Riga Technical University, Paula Valdena Street 3/7, Room 272.

OFFICIAL REVIEWERS

Professor Sergejs Gaidukovs
Riga Technical University

Dr. Antons Sizovs
Latvian Institute of Organic Synthesis

Professor Jagoda Litowczenko-Cybulska
Adam Mickiewicz University in Poznań, Poland

DECLARATION OF ACADEMIC INTEGRITY

I hereby declare that the Doctoral Thesis submitted for review to Riga Technical University for promotion to the scientific degree of Doctor of Science (Ph. D.) is my own. I confirm that this Doctoral Thesis has not been submitted to any other university for promotion to a scientific degree.

Abhishek Rajesh Indurkar ……. (signature)
Date: ……

The Doctoral Thesis has been prepared as a thematically united collection of scientific publications. It consists of a summary in Latvian and English and eight publications. The publications are written in English and include electronically available supplementary information.

TABLE OF CONTENTS

ACKNOWLEDGEMENT

I want to express my sincere gratitude to the individuals who have been instrumental in completing the Thesis, providing unwavering support, gratitude, and encouragement.

To my esteemed co-authors, your contribution and shared commitment to the research have significantly enhanced the depth and quality of this Thesis. Your contribution has been invaluable, and I am grateful for the collective efforts.

My heartfelt thanks to my supervisors for their expert guidance, mentorship, and patience. Their insights and encouragement have been pivotal in shaping the course of my research journey.

To my parents, your unwavering support and belief in my abilities have been a constant source of motivation. Your sacrifices and encouragement have laid the foundation for my academic pursuits. I am deeply grateful to my wife for her enduring support, understanding, and encouragement throughout this challenging yet fulfilling journey. Your presence is my anchor, and I am blessed to share this accomplishment with you.

Finally, I want to acknowledge God's divine guidance and blessings. The strength and resilience I found in the challenging moments was a testament to His grace.

In conclusion, thanks to everyone who has played a role in the academic endeavor. Your collective contribution and support made this journey meaningful and rewarding.

LIST OF ABBREVIATIONS

SOM – Small Organic Molecules
CaP – Calcium Phosphate
Ap – low crystalline apatite
HA – hydroxyapatite
ACP – Amorphous Calcium Phosphate
ACP_CL – amorphous calcium phosphate without any organics
ACP_NIT – amorphous calcium phosphate without any organics
ACP_ACE – acetate-containing amorphous calcium phosphate
ACP_ASC – ascorbate-containing amorphous calcium phosphate
ACP_CIT – citrate-containing amorphous calcium phosphate
ACP_GLU – glutamate-containing amorphous calcium phosphate.
ACP_ITN – itaconate-containing amorphous calcium phosphate.
ADA-GEL – alginate-dialdehyde-gelatin
SN – Single-Network
DN – Double-Network
DI – Deionized
PBS – Phosphate Buffer Saline
α-MEM – Minimum Essential Medium Eagle – alpha modification
P123 – Pluronic P123
GELMA – gelatin methacrylate
PAM – polyacrylamide
APS – ammonium persulfate
TEMED – Tetramethylethylenediamine
MSC – Mesenchymal Stem Cells
FBS – Fetal Bovine Serum

GENERAL OVERVIEW OF THE THESIS

INTRODUCTION

Globally, over 4.5 million reconstructive surgeries are conducted each year to address a range of causes, including accidents, cancer procedures, and cosmetic enhancements [1]. Global Burden Disease data analysis revealed that approximately 1.71 billion people worldwide have musculoskeletal conditions [2]. Consequently, there is a need for effective biomaterial for bone treatment and replacement. The unique characteristics of bone, its constituent phases, and structural relationships at various hierarchical levels are complex. Therefore, replicating it artificially to achieve biomaterials with properties comparable to bone has proven challenging [3].

For this reason, allograft remains a gold standard for treating bone-related disorders [4]. There is a need to develop synthetic materials similar to natural bone [5]. Bone is a nanocomposite material made up of inorganic and organic counterparts. The organic component primarily comprises calcium phosphate (CaP), while the organic content predominantly comprises collagen.

The inorganic content of bone is synthesized through a mitochondrial-dependent cellular mechanism in the form of amorphous calcium phosphate (ACP), which is further nucleated to low-crystalline apatite (Ap) in the presence of collagen [6]. In mitochondria, the ACP is associated with an organic compound that regulates interfibrillar collagen mineralization. The side chains of an organic compound (carboxylate or hydroxyl groups) allow interaction with CaP by surface adsorption [7]. The organic compound delay CaP crystallization can be due to retarding the transformation rate (crystallization) of ACP to Ap or interaction with the crystalline phase by inhibiting the growth of nuclei. Therefore the organic compound becomes a key player in regulating interfibrillar collagen mineralization [8]. The Doctoral Thesis aims to develop small organic molecule-containing ACPs and their nanocomposites as bone substitute materials for improved bone regeneration. Based on this, five synthetic SOMs have been selected with diverse functional groups and used for the development of SOM-containing ACPs. These SOMs are also naturally present in mitochondria and play a role in bone regeneration.

The primary goal was to develop a wet chemical synthesis route for the synthesis of SOM-containing ACP and analyze the impact of SOM on ACP's physiochemical properties (particle size, morphology, true density, specific surface area, and transformation kinetics) and cytocompatibility. Synthetic SOM-containing ACPs were used as inorganic fillers in an organic matrix to develop nanocomposite scaffolds.

Nanocomposite bioink was developed by adding the SOM-containing ACPs as an inorganic filler in an alginate-dialdehyde-gelatin (ADA-GEL) organic matrix wherein citrate-containing ACP (ACP_CIT) was effective in maintaining the structural integrity of the bioprinted scaffolds. Subsequently, a single-network (SN) nanocomposite hydrogel consisting of gelatin methacrylate (GELMA) and ACP_CIT was developed using chemical crosslinking.

Afterwards, a double network (DN) nanocomposite hydrogel of polyacrylamide (PAM), Pluronic P123, GELMA, and ACP_CIT was formulated. Initially, the effect of P123 on the mechanical properties of PAM-GELMA hydrogel was evaluated, followed by analyzing the effect of ACP on the mechanical and rheological properties of PAM-GELMA-P123 hydrogels. Subsequently, their shape memory effect was also evaluated. In conclusion, all the synthesized ACPs and their nanocomposite

bioink, SN, and DN hydrogels demonstrate cytocompatibility, suggesting their potential use in bone tissue regeneration applications.

THE AIM OF THE THESIS

The Thesis aimed to develop SOM-containing ACPs, investigate their physiochemical characteristics and cytocompatibility, employ them as fillers in nanocomposite development, and assess their mechanical and rheological properties. The following tasks were set to fulfil the aim:

1. To develop a wet chemical route for the synthesis of SOM-containing ACP.
2. To examine the influence of SOM on the physiological properties and transformation kinetics of ACP to low-crystalline apatite (Ap) in aqueous media: deionized (DI) water, PBS and α-MEM cell culture media.
3. To incorporate developed ACPs into bioink, SN, and DN hydrogel and investigate the properties of developed nanocomposites.

THESIS TO DEFEND

1. Incorporating SOM in ACP influences its physiochemical properties, transformation kinetics, and cytocompatibility.
2. Solution-mediation transformation of ACP to Ap is affected by the composition of aqueous media (deionized water, PBS, and α-MEM cell culture media).
3. The addition of ACP filler in bioink, SN, and DN hydrogels enhances their rheological, mechanical, and structural properties while maintaining cytocompatibility.

SCIENTIFIC NOVELTY

1. A one-step wet chemical approach was developed to synthesize pure and SOM-containing ACP (such as acetate, ascorbate, citrate, itaconate, and glutamate).
2. New ACPs with acetate, ascorbate, and itaconate were synthesized.
3. For the first time, the influence of SOM on the transformation kinetics of ACP to Ap in different aqueous mediums was evaluated.
4. Novel nanocomposite bioink, SN and DN hydrogel containing ACP were developed.
5. A new formulation of PAM-GELMA-P123 hydrogel was created.

PRACTICAL SIGNIFICANCE

1. The developed synthesis methods can be expanded to include other SOMs in ACP.
2. The transformation kinetics of ACP to Ap can be tailored using a combination of specific SOM and aqueous media for specific applications.
3. DN hydrogel with tailored mechanical properties can be developed by modulating the concentration of P123 in PAM-GELMA hydrogel.

STRUCTURE OF THE THESIS

1. The Thesis is created as a thematically unified set of scientific papers which focus on developing SOM-containing ACPs and their nanocomposites (bioink, SN, and DN hydrogel). Each paper stands on its own, presenting new knowledge and original research. Together, the papers form an extensive long-term body of research to create a new approach for synthesizing SOM-containing ACP and developing its nanocomposites.
2. The study began with an in-depth literature review (***Publication 1)*** to understand the physical properties, biological occurrence, and synthesis of various calcium phosphate (CaP) types and their use as bone substitute materials. The examination revealed that achieving pure crystalline CaP requires high-temperature synthesis or treatments. Amorphous calcium phosphate (ACP) is a metastable form of calcium phosphate; therefore, densification at high temperature is not possible.
3. In ***Publication 2,*** ACP was synthesized using the dissolution precipitation method. The obtained ACP powder was sintered to near full density by simple uniaxial pressing at 1250–1500 MPa at room temperature maintaining the amorphous nature.
4. Naturally, the bone apatite is nonstoichiometric and structurally disordered. Therefore, *Publication 3*, focused on understanding the mechanism of bone apatite formation and the role of collagen and organic molecules in regulating mineralization. Naturally, ACP is formed through a mitochondrial-dependent cellular mechanism. Additionally, ACP is associated with an organic compound in the mitochondria. The side chains of organic compounds (carboxyl and hydroxyl groups) regulate Ap nucleation and collagen interfibrillar mineralization. The organic compounds' capability depends on the number of functional groups at specific configurations. Therefore, five SOMs were selected based on different functional groups, natural presence in mitochondria, and role in bone physiology. The primary goal of the Doctoral Thesis was to synthesize the SOM-containing ACP**.**
5. In ***Publication 4***, the focus is on developing a one-step wet chemical approach for the synthesis of pure, acetate (ACP_ACE), and citrate-containing ACP (ACP_CIT). The synthesis approach developed in ***Publication 4*** was further used to synthesize glutamate (ACP_GLU), itaconate (ACP_ITN), and ascorbate-containing ACP (ACP_ASC) in ***Publication 5.*** All the synthesized ACPs were characterized, and the results have shown the impact of SOM on the physiochemical properties and cytocompatibility of ACP.
6. In ***Publication 6,*** the effect of ACP's particle size, transformation kinetics, and SOM on ADA-GEL hydrogel and printed scaffold were analyzed. ACP_ACE and ACP_CIT were used as an inorganic filler in the ADA-GEL organic matrix for developing nanocomposite hydrogels. Nanocomposite bioinks were developed by adding MC3T3-E1 cells in the ACP-ADA-GEL hydrogels. Both bioinks comprising ACP_CIT and ACP_ACE were cytocompatible; however, the ACP_CIT was more effective in maintaining the structural integrity of the printed scaffolds.
7. In ***Publication 7,*** a nanocomposite SN hydrogel of ACP_CIT and GELMA was developed using a chemical crosslinking approach using APS/TEMED as an alternative to photo-crosslinking. *In vitro* analysis has confirmed that the chemical crosslinking and incorporation of ACP_CIT did not hamper the cytocompatibility of GELMA hydrogel.

8. In ***Publication 8***, a DN thermoresponsive hydrogel consisting of PAM-GELMA-P123 was synthesized. The primary network of DN hydrogel was developed using P123, while the secondary network consisted of a co-polymer of PAM-GELMA. Both the PAM-GELMA were chemically crosslinked using APS/TEMED. Initially, the concentration of P123 in PAM-GELMA hydrogel was adjusted to achieve optimum mechanical properties. Afterwards, the effect of different concentrations of ACP_CIT on the mechanical properties of PAM-GELMA-P123 hydrogel was analyzed. Additionally, the shape memory effect of the nanocomposite DN hydrogel was examined.

LIST OF APPENDED PAPERS

RESULTS OF THE THESIS WERE PUBLISHED IN SCI SCIENTIFIC PUBLICATIONS

Published

1. **Indurkar, A.,** Choudhary, R., Rubenis, K., & Locs, J. (2021). Advances in sintering techniques for calcium phosphates ceramics. Materials, 14(20), 6133. doi.org/10.3390/ma14206133 (Scopus, Open Access, IF 3.4, Q2, CiteScore 5.2). (***Publication 1***).
2. Rubenis, K., Zemjane, S., Vecstaudza, J., Lazdovica, K., Bitenieks, J., Wiecinski, P., **Indurkar, A.,** & Locs, J. (2022). Sintering of amorphous calcium phosphate to near-full density by uniaxial compaction at room temperature. Journal of the European Ceramic Society, 42(13), 6199–6205. doi.org/10.1016/j.jeurceramsoc.2022.06.041 (Scopus, Open Access, IF 5.7, Q1, CiteScore 10.1) (***Publication 2***)
3. **Indurkar, A.,** Choudhary, R., Rubenis, K., & Locs, J. (2023). Role of carboxylic organic molecules in interfibrillar collagen mineralization. Frontiers in Bioengineering and Biotechnology, 11, 1150037. doi.org/10.3389/fbioe.2023.1150037 (Scopus, Open Access, IF 5.7, Q1, CiteScore 6.7) (***Publication 3***)
4. **Indurkar, A.,** Choudhary, R., Rubenis, K., Nimbalkar, M., Sarakovskis, A., Boccaccini, A. R., & Locs, J. (2023). Amorphous calcium phosphate and amorphous calcium phosphate carboxylate: Synthesis and characterization. ACS Omega. doi.org/10.1021/acsomega.3c00796 (Scopus, Open Access, IF 4.1, Q1, CiteScore 5.9) (***Publication 4***)
5. **Indurkar, A.,** Kudale, P., Rjabovs, K., Heinmaa, I,. Demir, O., Kirejevs, M., Rubenis, K., Chaturbhuj, G., Turka, M., & Locs, J. (2023). Small Organic Molecules Containing Amorphous Calcium Phosphate: Synthesis, Characterization and Transformation. Frontiers in Bioengineering and Biotechnology, 11. doi.org/10.3389/fbioe.2023.1329752 (Scopus, Open Access, IF 5.7, Q1, CiteScore 6.7) (***Publication 5***)

In press (Under review)

1. **Indurkar, A.,** Heid, S., Bauer, J., Rubenis, K., Friedrich, O., Locs, J., & Boccaccini, A. R. Amorphous Calcium Phosphate Reinforced Alginate-Dialdehyde-Gelatin (Ada-Gel) Bioinks for

Biofabrication of Bone Tissue Scaffolds (Under review in Scientific reports) (Scopus, Open Access, IF 4.6, Q1, CiteScore 6.9). (***Publication 6***)

2. **Indurkar, A.,** Rubenis, K., Boccaccini, A. R., & Locs, J. Development of nanocomposite hydrogel using citrate-containing amorphous calcium phosphate and gelatin methacrylate (Under review in Frontiers in Bioengineering and Biotechnology) (Scopus, Open Access, IF 5.7, Q1, CiteScore 6.7) (***Publication 7***)
3. **Indurkar, A.,** Rubenis, K., Boccaccini, A. R., & Locs, J. Development and Characterization of Thermoresponsive Double-Network Nanocomposite Hydrogel for Bone Tissue Engineering (Under review in Macromolecular Materials and Engineering) (Scopus, Open Access, IF 3.9, Q1, CiteScore 6.5) (***Publication 8***)

RESULTS OF THE THESIS PRESENTED AT SCIENTIFIC CONFERENCES

1. Development of nanocomposite double network hydrogel: Vecstaudza, J., Egle, K., **Indurkar, A.,** Locs, J. 64th International Scientific Conference of Riga Technical University, Latvia held on 6th October 2023. (***Oral presentation***)
2. Development of nanocomposite double network hydrogel: **Indurkar, A.,** Rubenis, K., Boccaccini, A. R., & Locs, J. 64th International Scientific Conference of Riga Technical University, Latvia, held on 6th October 2023. (***Oral presentation***)
3. Amorphous calcium phosphate citrate reinforced gelatin-alginate dialdehyde bioink for bone regeneration: **Indurkar, A.,** Rubenis, K., Boccaccini, A. R., & Locs, J. International Conference on Biofabrication, Saskatoon, Canada, held on 17th to 20th September 2023. (***Oral presentation***)
4. Amorphous calcium phosphate citrate reinforced gelatin-alginate dialdehyde bioink for bone regeneration: **Indurkar, A.,** Rubenis, K., Boccaccini, A. R., & Locs, J. FEMS EuroMat 2023, Frankfurt, Germany,held on 3rd to 7th September 2023. (***Oral presentation***)
5. Amorphous calcium phosphate citrate reinforced gelatin-alginate dialdehyde bioink for bone regeneration: **Indurkar, A.,** Rubenis, K., Boccaccini, A. R., & Locs, J. 5th World Congress of Latvian Scientists, Riga, Latvia, held on 26th to 29th June 2023. (***Poster presentation***)
6. Biomimetic synthesis of amorphous calcium phosphate: **Indurkar, A.,** Choudhary, R., Rubenis., & Locs, J. 16th Scandinavian Society of Biomaterials, Røros, Norway held on 21st to 24th March 2023. (***Poster presentation***)
7. Tailor-made synthesis of bionic amorphous calcium phosphate: **Indurkar, A.,** Choudhary, R., Rubenis, K., Locs, J. Biomaterials and novel technologies for healthcare 3rd biennial International Conference BIOMAH, Rome, Italy, held on 18th to 21st October 2022. (***Oral presentation***)

INDIVIDUAL CONTRIBUTION TO PAPERS

The papers discussed in this Thesis are co-authored with 16 collaborators and supervised by experienced mentors who provided strong support and valuable input. The author of the Thesis played a pivotal role in each paper, shaping the research and exploring background literature. The author of the Thesis focused on developing a one-step wet chemical approach for synthesizing ACP (with and without SOM) and its characterization. The developed ACPs were used to create nanocomposite bioink, SN, and DN hydrogel.

During the Doctoral Thesis, the author had interactive discussions with the co-authors and supervisors, which has proven vital for overcoming hurdles and navigating the complexity of the research. The collective process has kept the author actively involved with his team. While the author's work and theirs are distinct, all the co-authors and supervisors have propelled the study in this field forward.

RESEARCH ROADMAP

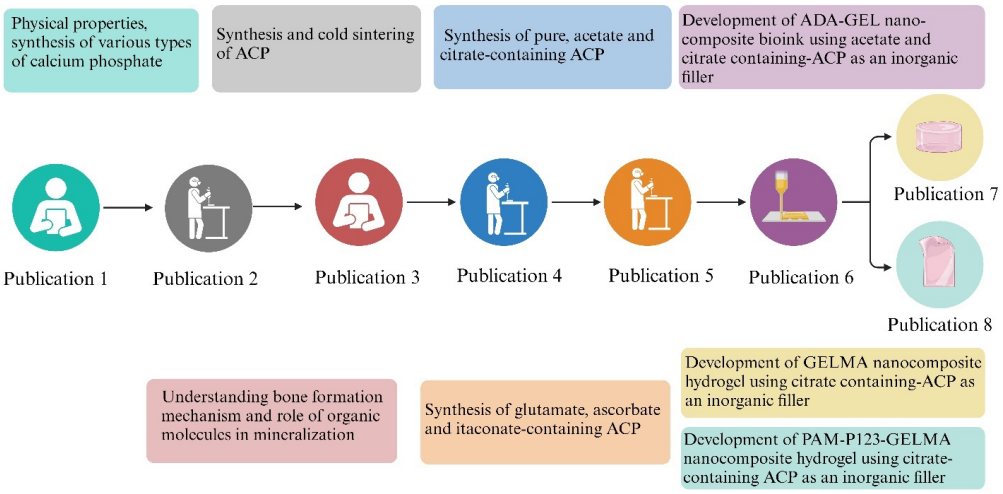

Fig. 1. Roadmap of appended papers for developing SOM-containing ACP and its nanocomposites bioink, SN, and DN hydrogels.

THE MAIN RESULTS OF THE THESIS

LITERATURE SURVEY

Bone is a dense form of connective tissue (osseous tissue) that constitutes the fundamental framework of the human skeletal system. Osseous tissue comprises specialized cells and a matrix comprising 65–70 % biomineral by weight and 5–8 % water, with the rest including organic materials [9]. The mineral phase mainly comprises CaP, the principal component being carbonated hydroxyapatite (cHA). The organic matrix comprises 90 % collagen and 10 % non-collagenous proteins.

CaP is a significant component in bone. In past decades, various CaP biomaterials have been used in bone regeneration studies and clinical applications [10]. Therefore, Publication 1 highlighted a comprehensive overview of CaP materials, such as their physical properties, biological occurrences, and diverse synthesis methods [11]. The examination revealed that achieving pure crystalline CaP requires high-temperature synthesis or treatments, encouraging to review numerous sintering methods for obtaining pure and stoichiometric CaP materials.

Synthetic hydroxyapatite (HA) developed under high temperatures has the chemical formula $Ca_{10}(PO_4)_6(OH)_2$. However, bone apatite formed at low temperatures is not well crystalline and termed

a low or poorly crystalline form of calcium apatite that is structurally disordered and nonstoichiometric due to the presence of one or more cationic (Na^+, K^+, Fe^{2+}, Mg^{2+}, Zn^{2+}, Sr^{2+}) and/or anionic (HPO_4^{2-}, CO_3^{2-}, Cl^-, F^-, citrate) species [12]. Such impurities in bone apatite introduce stress into the crystal structure, making it less stable and more reactive [13]. Moreover, bone apatite has a unique geometry where the length does not exceed 30–50 nm while maintaining a thickness close to 2 nm [14]. Therefore, Publication 3 focused on understanding the mechanism of bone apatite formation [15].

The organic component of bone plays a vital role in apatite formation. ACP is the first solid phase of CaP formed by mitochondrial-dependent cellular mechanisms. ACP is associated with an organic compound (Howard factor) in mitochondria, indicating a complex inorganic-organic formation. This complex is transferred onto the collagen matrix, where ACP transforms to low crystalline apatite (Ap).

The organic component of bone plays a crucial role in Ap formation. In bone, collagen is arranged in a parallel staggered array, as shown in Fig. 2. The collagen molecules are shifted by distance D, wherein one D-repeat consists of a complete collagen sequence of 67 nm, and the distance between two tropocollagen subunits measures 40 nm, termed as the gap zone [16]. The gap zone serves as a nucleation site for ACP to Ap transformation, wherein Ap achieves its c-axis orientation parallel to the long axis of collagen [17].

However, previous studies have shown that synthetic combinations of ACP/collagen cannot initiate apatite nucleation [18]. Therefore, it was clear that collagen alone cannot initiate mineralization independently, and a nucleation catalyst regulating the process is present. The nucleation catalyst is an organic molecule of specific reactive side chains (carboxyl or hydroxyl groups) arranged in a stereochemical array [8].

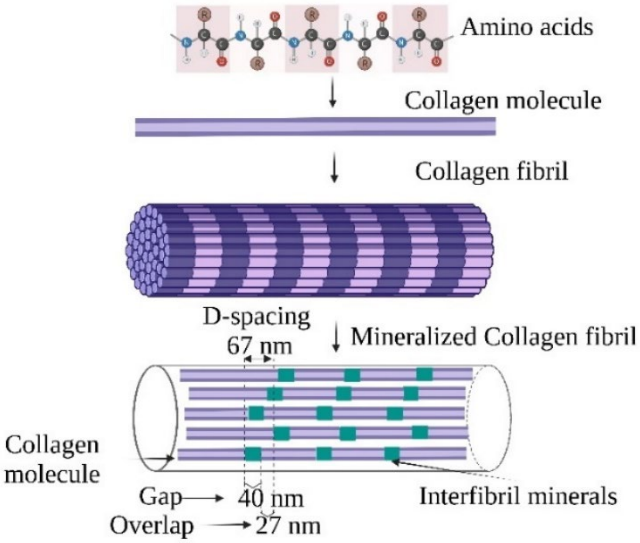

Fig. 2. Schematic illustration of the hierarchical structure of collagen.

Poly-aspartate was the first organic compound analyzed for collagen interfibrillar mineralization. Adding poly-aspartate improves the connection between CaP and collagen, creating separate CaP crystals in the collagen fibril. On the contrary, the absence of poly-aspartate resulted in clusters of CaP crystals loosely bound to collagen fibril. Poly-aspartate interacts with CaP by surface adsorption, and the delay of CaP crystallization can be due to retarding the transformation rate of ACP to Ap or due to

interaction with the crystalline phase by inhibition growth of nuclei [7]. This study established the fundamental significance of organic molecules in regulating collagen interfibrillar mineralization.

Subsequently, further research was focused on analyzing different organic molecules (non-collagenous proteins, polymers, and small organic molecules) in developing synthetic CaP. The list of the organic molecules used in developing CaP is highlighted in Publication 3.

SELECTION OF SMALL ORGANIC MOLECULES

Naturally, ACP is formed through a mitochondrial-dependent cellular mechanism, as illustrated in Fig. 3 A). Furthermore, ACP forms a complex with an organic compound in the mitochondria. The literature showed that the side chains of organic compounds (carboxyl and hydroxyl groups) can induce apatite nucleation [5]. The functional groups should have the required configuration to induce CaP nucleation under stimulated body conditions. Therefore, in this study, selected five synthetic SOMs have been selected that are also naturally present in mitochondria. These SOMs play a role in bone regeneration and have different functional groups, as shown in Fig. 3 B).

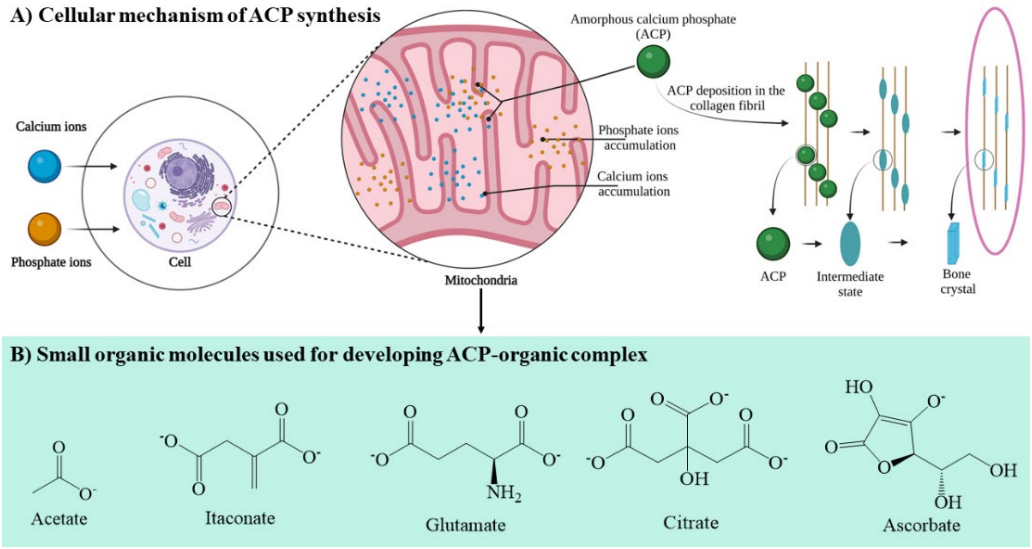

Fig. 3. A) – Formation of ACP by mitochondrial-dependent cellular mechanism. B) – Synthetic SOMs that are also naturally present in mitochondria are used to synthesize SOM-containing ACP.

Acetate is a monocarboxylic compound that enhances stem cell differentiation by increasing histone acetylation and chromatin assembly. Bone marrow mesenchymal stem cells (MSCs) regulate bone regeneration by giving rise to adipocytes, chondrocytes, and osteoblasts. However, aged MSCs have a decreased capacity to differentiate into osteogenic and chondrogenic linage. Treatment of aged MSC by supplementing acetate rescues the osteogenic defects of aged MSC [19].

Itaconate and glutamate are dicarboxylic compounds present in mitochondria. Itaconate is a metabolite that regulates osteoclast differentiation and activation, maintains bone homeostasis, and reduces inflammatory bone loss caused by lipopolysaccharide-induced inflammation [20]. Glutamate is a fundamental extracellular messenger molecule used for neural and non-neural signaling in bone. The osteoblasts, osteoclasts, and bone marrow cells express the glutamate receptors. Activation of glutamate receptors controls the phenotype of osteoblasts and osteoclasts *in vitro* and bone mass *in vivo* [21]. Moreover, glutamate has attained the nitrogen balance in a fractured bone, thus accelerating the bone healing process [22].

Citrate is a tricarboxylic compound and an essential component synthesized in the Kerbs cycle. In 1941, the presence of citrate in bone was first identified [23]. The citrate concentration in bones is 20–80 µmol/g, which is 100–400 folds higher than in most soft tissues. Bone comprises 1.6 % citrate, and

about 90 % of body citrates are found in human bone [24]. Recent NMR studies have shown the presence of citrate in bone [25]. The complex interaction of the citrate with the apatite regulates the Ap's lattice orientation, particle size, and distribution. The long axis of the citrate molecule is parallel to the surface of the apatite. The three carboxylic groups of citrates are at 0.3–0.45 nm from the apatite surface. The spacing of the carboxylic groups matches with the calcium ion along the c-axis of the apatite. Therefore, the crystal growth is inhibited in the direction of thickness but continued in the longitudinal direction [26].

Ascorbate (vitamin C) is crucial in collagen synthesis and is a vital organic compound in connective tissues and bone [27]. Collagen provides structure and flexibility to the bone, enabling it to withstand mechanical stress. Without sufficient ascorbate, collagen synthesis is impaired, weakening the bone structure and increasing susceptibility to bone fractures [28]. Furthermore, osteogenic cell differentiation depends on ascorbate [29], [30].

In summary, SOMs such as acetate, itaconate, glutamate, citrate, and ascorbate play a crucial role in bone physiology. Therefore, these SOMs were used to synthesize SOM-containing ACP, and the effect of different functional groups on the physiochemical properties of ACP and cytocompatibility was analyzed.

SYNTHESIS OF ACP WITH SOM

Initially, the dissolution precipitation method was used to synthesize ACP in one step involving the dissolution of hydroxyapatite and rapid addition of alkali (***Publication 2***), as depicted in Fig. 4 A). However, previous studies have performed the synthesis of SOM-containing ACP by a multi-step approach wherein the SOM was either introduced in its acidic or basic form, as illustrated in Fig. 4 B). Therefore, the aim was to develop a one-step approach to synthesize ACP both with and without SOM.

The complicated step in ACP synthesis is the triprotic nature of phosphate ions. In an acidic solution, ACP contains HPO_4^{2-} instead of PO_4^{3-} therefore compromising the synthesized product (ACP) [31]. ***Boskey and Posner*** have proved the influence of factors such as synthesis pH, surface area, calcium concentration, stirring rate, and slurry concentration on the physiochemical characteristics of synthesized ACP under consistent temperature conditions at 26 °C. The effect of the synthesis pH of ACP on the transformation time to apatite is shown in Table 1.

Table 1

Effect of Synthesis pH on ACP Transformation to Apatite [32]

ACP synthesis pH	Time needed for ACP transformation to apatite (min)
6.8	16
7.0	30
7.5	48
8.0	120
9.0	135
10.0	280

The literature describes various approaches to synthesize pure and SOM-containing ACP. Different approaches have different synthesis parameters, such as pH, stirring rate, reaction time, volume, and

calcium and phosphate ion concentrations. Therefore, comparing pure and SOM-containing ACP becomes problematic when using different synthesis parameters.

In the Doctoral Thesis, a one-step wet chemical synthesis approach of pure and SOM-containing ACP was developed, keeping constant synthesis parameters such as synthesis pH, reaction volume, temperature, stirring rate, and calcium and phosphate ions concentrations. This standardized approach allows us to analyze the effect of SOM on ACP's physiological properties.

The synthesis approach described in Publication 4 for the pure ACP employed the following strategy: calcium chloride or calcium nitrate solutions (150 mM in 150 ml Milli-Q® water) were prepared, and their pH was adjusted to 11.5 using 3M NaOH solution, followed by the addition of an equal amount of trisodium phosphate (100 mM in 150 ml Milli-Q® water) under constant stirring of 500 rpm, as illustrated in Fig. 4 C).

Similarly, for the synthesis of SOM-containing ACP (***Publications 4 and 5***), (150 mM) calcium acetate, (50 mM) calcium citrate, or (150 mM) calcium glutamate was added in 150 ml Milli-Q® water. Their pH was adjusted to 11.5 using 3M NaOH solution, followed by adding an equal amount of trisodium phosphate (100 mM in 150 ml Milli-Q® water) under constant stirring of 500 rpm, as illustrated in Fig. 4 D).

The process for itaconate and ascorbate-containing ACP followed a similar approach, as shown in Fig. 4 D). Calcium chloride (150 mM) and itaconic anhydride (150 mM) or ascorbic acid were added to 150 ml Milli-Q® water. Their pH was adjusted to 11.5 using 3M NaOH solution, followed by adding an equal amount of trisodium phosphate (100 mM in 150 ml Milli-Q® water) under constant stirring of 500 rpm.

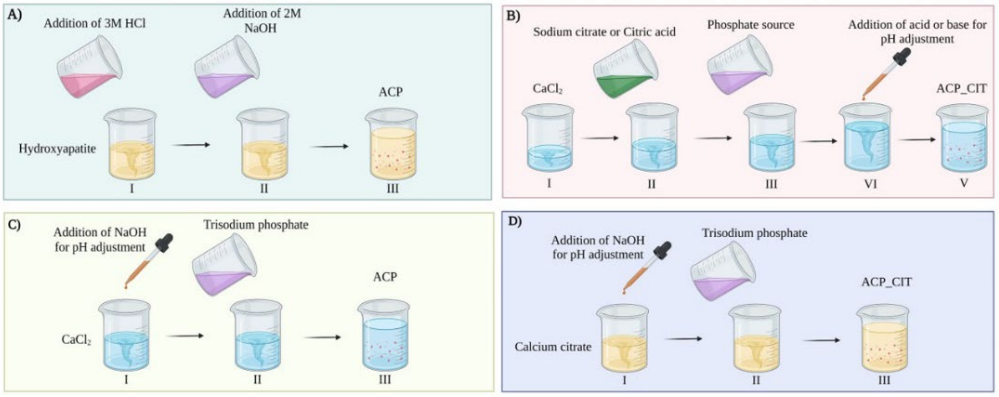

Fig. 4. Traditional synthesis approach for pure ACP (A) and SOM-containing ACP (B). The synthesis approach in which the pH of the calcium chloride solution was adjusted to 11.5 using 3M NaOH, followed by adding trisodium phosphate (C). SOM was consumed as calcium salt, making pH adjustment convenient with marginal pH variation after adding trisodium phosphate (D).

In every synthesis method, the pH of the calcium salt (with or without SOM) was set to 11.5 using 3M NaOH, and trisodium phosphate inherently had a pH of 12. The reaction pH stayed between 10.5 and 11.5 when these solutions were mixed. Moreover, the synthesis reaction volume, temperature, stirring rate, calcium and phosphate ions concentrations, and the downstream process (centrifuge, washing thrice with Milli-Q® water, liquid nitrogen freeing of precipitate, and lyophilization) were the same. As a result, pure and SOM-containing ACPs were produced under similar conditions, enabling

a comparison between them. Moreover, it also allows examining the effect of SOM on physiochemical properties and transformation kinetics of ACP to Ap.

PHYSIOCHEMICAL PROPERTIES OF SYNTHESIZED ACP VARIANTS

Publication 4 outlines the physiochemical characteristics of synthesized pure ACP as well as ACP_CIT and acetate-containing ACP (ACP_ACE). At the same time, ***Publication 5*** provides information on ascorbate (ACP_ASC), glutamate (ACP_GLU), and itaconate-containing ACP (ACP_ITN).

The XRD analysis of all the synthesized ACP variants shows a broad featureless background, showing an X-ray amorphous nature. The splitting in the $v_4\ PO_4^{3-}$ vibration region (500–620 cm^{-1}) in FTIR spectra is not seen, thus confirming the amorphous nature of all the synthesized ACP variants.

The solid-state ^{31}P nuclear magnetic resonance (NMR) analysis of all ACP variants has shown a characteristic broad Gaussian peak centered from 2.2 ppm to 6.5 ppm, corresponding to ACP. The functional groups of ACP and respective SOM were confirmed using FTIR and solid-state ^{13}C nuclear magnetic resonance (NMR) analysis.

The morphology of ACP observed in zebrafish fin, embryonic chicken long bones, and developing mouse calvaria were either spherulite or globular, with particle sizes ranging from 10–50 nm [33], [34]. Figure 5 displays the TEM analysis of the synthesized and SOM-containing ACP variants.

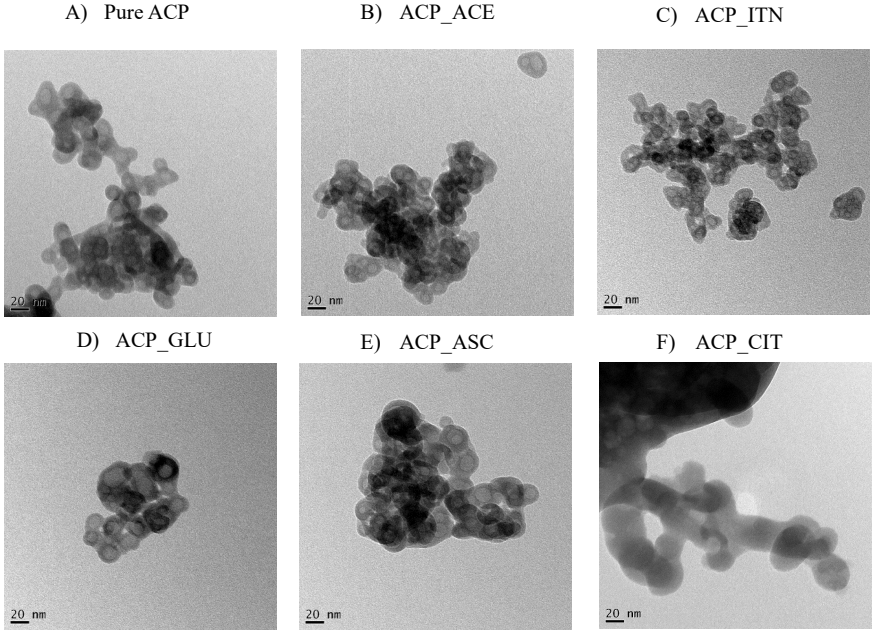

Fig. 5. Morphology and particle size analysis of all the synthesized ACP variants (scale bar of 20 nm): A) – pure ACP, B) ACP_ACE (acetate-containing ACP); C) – ACP_ITN (itaconate-containing ACP); D) – ACP_GLU (glutamate-containing ACP; E) – ACP_ASC (ascorbate-containing ACP); and F) – ACP_CIT (citrate-containing ACP).

The pure ACP, ACP_ACE, ACP_ASC, ACP_GLU, and ACP_ITN have a hollow spherical morphology with particle sizes close to 20 nm. On the other hand, ACP_CIT shows globular morphology with particle size close to 40 nm.

The effect of SOM on ACP's true density and specific surface area is shown in Table 2. The SOM used in this study possesses different functional groups. For instance, acetate is monocarboxylic, glutamate and itaconate is dicarboxylic, citrate contains tricarboxylic and a hydroxyl group, and ascorbate has hydroxyl groups. Both calcium and phosphate ions in ACP can react with the carboxylate group of acetate, citrate, itaconate, and glutamate. Similarly, the hydroxyl group can react with both phosphate and calcium ions. The functional group variations offer diverse negative charges, which react differently with calcium and phosphate ions in ACP. Therefore, the effect of SOM was observed on ACP's morphology, particle size, density, and SSA of ACP.

Table 2

Density and SSA of Synthesized ACP Variants

Sample	True density (g/cm^3)	SSA (m^2/g)
Pure ACP	2.62	105
Acetate-containing ACP	2.47	118
Itaconate-containing ACP	2.43	130
Glutamate-containing ACP	2.64	92
Ascorbate-containing ACP	2.82	115
Citrate-containing ACP	2.57	62

CRYSTALLIZATION KINETICS OF SYNTHESIZED ACPS IN AQUEOUS MEDIUM

In vitro analysis is the primary measure to scrutinize the cellular responses of a material. This examination often involves the material's exposure to diverse solutions. Specifically, for ACP, which is recognized for its metastable nature, a comprehensive investigation of its transformation kinetics in an aqueous medium becomes crucial before evaluating the *in vitro* performance. Therefore, in ***Publication 5***, transformation kinetic experiments of all the synthesized ACPs were performed. The media used were DI water, PBS, and α-MEM medium.

In literature, earlier studies have discovered that the transformation kinetics of ACP to Ap is unaffected by the following factors: a) the nature of the buffer system used, b) the presence of different types of univalent ions, c) the ACPs were in contact with mother liquor or filtered, dried, or added to the fresh buffer. The parameters affecting the transformation kinetics are stirring rate, slurry composition, solvent type, presence of foreign ions, and additives (polyelectrolytes, phospholipids, polyglycols, proteins). In this context, the effect of SOM on ACP to Ap transformation has received relatively less attention [32].

The transformation experiments were initially performed in DI water, as shown in Fig. 6. Results revealed that the transformation of ACP_ACE to Ap was faster than pure ACP. The side chains of an organic compound (carboxylate or hydroxyl groups) allow interaction with CaP by surface adsorption. The functional groups in organic molecules possess different effects on the physiochemical properties of ACP (morphology, particle size, SSA, and true density of ACP).

NMR analysis has confirmed that pure ACP has carbonate ions with a negative charge of –2. Acetate consists of single carboxylic groups offering a negative charge of –1. Fluoride ions also have a negative charge of –1; therefore, the transformation of ACP to Ap was faster in the presence of fluoride-doped ACP than in pure ACP [35], [36]. The negative charge of –1 in acetate was attributed to the faster transformation of ACP_ACE to Ap. The presence of carbonate ions in ACP is known to retard its conversion to Ap [31]. Similarly, itaconate and glutamate are dicarboxylic compounds with a negative charge of –2 and may behave similarly to carbonate-substituted ACP. Therefore, the transformation rate of pure ACP, ACP_GLU and ACP_ITN was the same.

Citrate is a tricarboxylic compound that can interact with CaP in four ways. The first most accepted interpretation is the interaction of Ca^{2+} with the COO^-, a group of citrates. The second interpretation is the interaction of OH^- of citrate with the phosphate ions. The third possible occurs through the substitution of the phosphate group with citrate anion. The fourth prediction is the interaction of carboxylic groups with phosphate ions. The carboxylate group of citrate has a negative charge of –3 offering multiple interactions with ACP, which can be attributed to the retarded transformation rate of ACP_CIT. In the case of ascorbate anion, the transformation rate was slower than other ACP variants (except ACP_CIT). The ascorbate anion can react with ACP, which may result in complex formation, thus retarding its conversion to Ap.

In PBS, all the synthesized ACPs showed rapid transformation to Ap. Earlier studies have revealed that in the presence of PBS solution, the organic compounds are released from the surface of ACP due to ionic exchange with the phosphate groups in the medium. This leads to an elevated phosphate concentration in ACP, thus reducing stability and rapidly transforming to Ap [37]. The phosphate content in the α-MEM medium was less than in PBS. Therefore, the transformation kinetics were slower (except for the ACP_CIT).

In the case of ACP_CIT, the amorphous nature was kept up to 2880 min in the α-MEM medium. In literature, the interaction of serum albumin with citrate-stabilized gold nanoparticles forms a protein-rich layer around the particle. Similarly, the delayed transformation of ACP_CIT may be due to the interaction of negatively charged citrate with Fetal bovine serum (FBS) present in α-MEM medium [38], [39].

FTIR analysis confirmed that the functional groups of respective SOMs in the transformed Ap were retained. SOM-containing Ap can be developed by integrating the synthesis and transformation kinetics approaches.

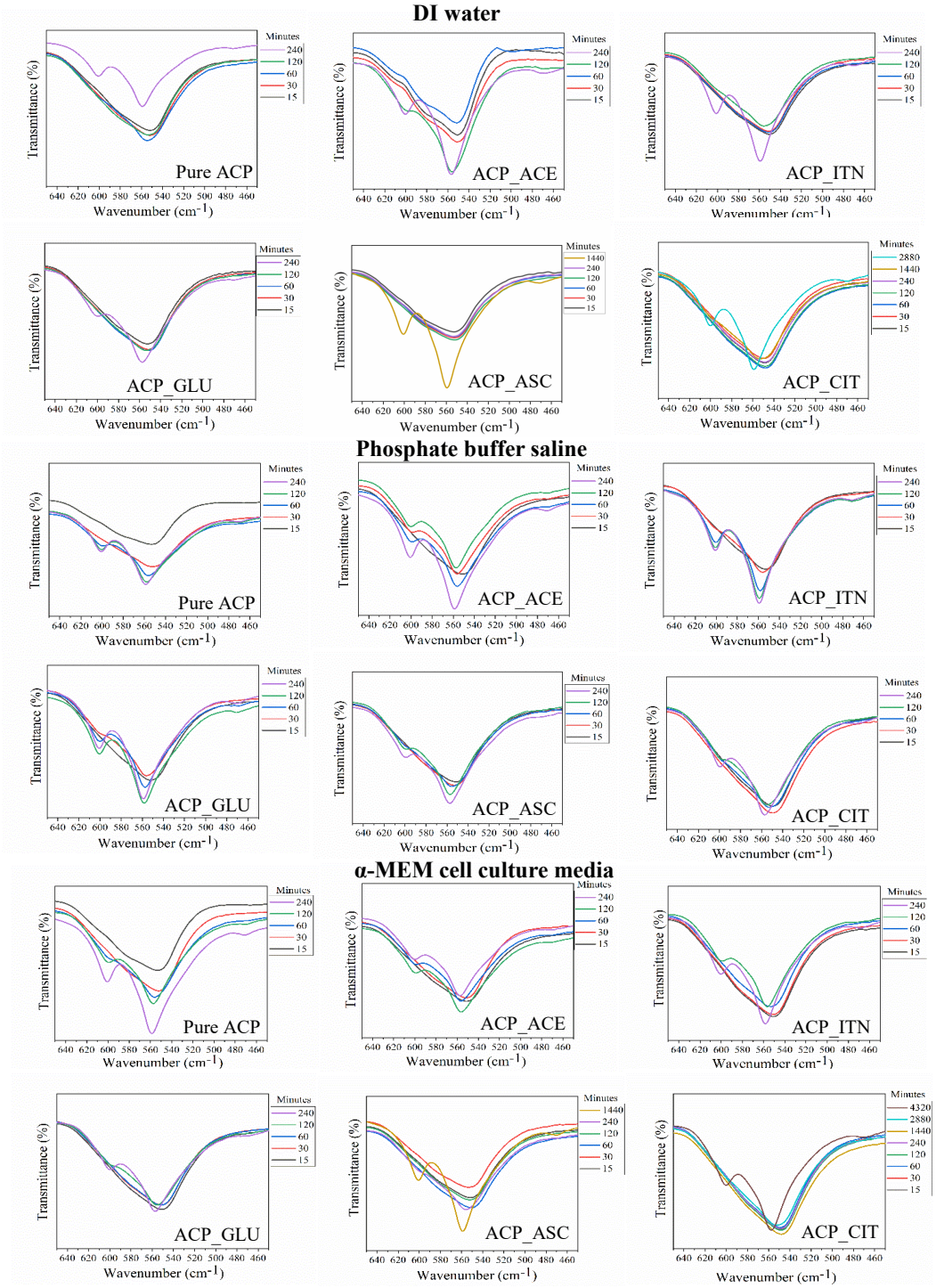

Fig. 6. Transformation kinetics of ACP to Ap in different aqueous mediums. The evaluation was based on v_4 PO_4^{3-} vibration region. The samples that did not show clear splitting in the v_4 PO_4^{3-} vibration region were termed amorphous; on the contrary, the samples that showed splitting of the v_4 PO_4^{3-} vibration region were termed low crystalline apatite.

IN VITRO ANALYSIS OF SYNTHESIZED ACPS

In vitro analysis of synthesized ACPs was performed with an osteoblast precursor cell line derived from mouse (Mus musculus) calvaria (MC3T3-E1). For cellular analysis, suspensions were prepared by adding 10 % w/v ACP precipitate in α-MEM medium and incubated at 37 °C in a humidified atmosphere of 95 % air and 5 % CO_2 for 24 h.

The extracts were collected by centrifugation and filtered to eliminate solid particles. The extracts were diluted with α-MEM medium to get the concentration of 1 % and 0.1 % w/v. For in-vitro analysis three concentrations were tested as follows: 10 %, 1 %, and 0.1 % w/v of each ACP variant. The extracts were then added to MC3T3-E1 containing well plates and incubated for 48 h. The α-MEM medium was added as a positive control. In contrast, the α-MEM medium with 6 vol% DMSO (dimethyl sulfoxide) was used as a negative control. The WST-8 (CCK-8, Sigma Aldrich) kit was used to analyze cell viability.

In ***Publication 4***, *in vitro* analysis of pure ACP, ACP_ACE and ACP_CIT was performed. The absorbance recorded from the positive control cells cultured in only medium was normalized to 100 %. The cells cultured with a 10 % w/v ACP_ACE extract showed the lowest cell viability. In contrast, the highest cell viability was observed in a 0.1 % w/v extract ACP_CIT. In the group of 10 % w/v, ACP_CIT has the highest cell viability, followed by pure ACP (ACP_CL and ACP_NIT) and ACP_ACE.

Since all the ACP samples shown in Fig. 7 exhibited cell viability of more than ~ 70 %, it can be inferred that all the samples were cytocompatible. *In vitro* analysis showed that ACP_CIT possesses maximum cell viability compared to other ACP samples (pure and ACP_ACE). This shows that the association of citrates enhanced the cell viability of ACP.

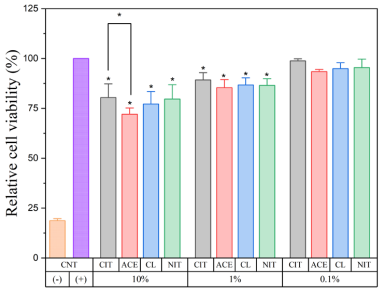

Fig. 7. Relative viability of MC3T3-E1 cells cultured with extract of different ACPs in 10 %, 1 %, 0.1 % w/v cell culture media dilutions (n = 12; CNT = control; samples in triplicate; *p < 0.05). The CL and NIT represent the pure ACP samples, while CIT and ACE represent citrate and acetate-containing ACP.

In ***Publication 5***, *in vitro* analysis of ACP_ASC, ACP_ITN and ACP_GLU was performed. The CNT+ and CNT– were positive and negative controls, respectively. Results revealed that the 10 % w/v ACP_GLU was cytotoxic. Higher glutamate concentration leads to excitotoxicity and or oxidative glutamate toxicity [40], [41]. However, reducing the concentration to 1 % w/v, ACP_GLU improved cell viability.

The 10 % w/v ACP_ITN and ACP_ASC concentration was better than 10 w/v% ACP_GLU. A similar trend was found in 1 w/v% ACP_ITN and ACP_ASC. The cell viability of 10 % and 1 % w/v ACP_ASC was better than CNT+.

Ascorbate is critical for the differentiation of the preosteoblast, and this may explain the higher cell viability [42], [43]. In conclusion, ACP samples (except 10 % w/v ACP_GLU), shown in Fig. 8, exhibited cell viability of more than ~ 70 %. It can be inferred that all the samples were cytocompatible.

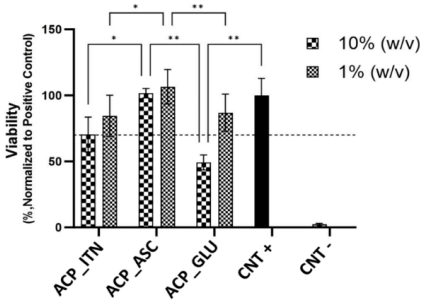

Fig. 8. Relative cell viabilities of MC3T3-E1 cells cultured with extracts of ACP variants (10 % and 1 % w/v) prepared in α-MEM medium. All the samples were analyzed in triplicate, and data is presented in average and standard deviation. The CNT+ and CNT– were positive and negative controls, respectively.

NANOCOMPOSITE BIOINK

The nanocomposite bioink containing ACP was designed for the first time. To analyze the effect of particle size, transformation kinetics, and respective SOM-containing ACP on the printed constructs' bioink properties and structural integrity, citrate and acetate-containing ACP were used for the nanocomposite bioink development.

In ***Publication 6***, bioprinting of the nanocomposite scaffold was performed in three stages: pre-printing, printing, and post-printing analysis.

In the pre-printing stage designing approach, scaffold material and cells were selected. Two nanocomposite bioinks were developed by incorporating ACP_CIT and ACP_ACE in the alginate-dialdehyde and gelatin (ADA-GEL) organic matrix.

GEL is a single-stranded protein obtained from the hydrolytic degradation of collagen. It consists of a large number of glycine, proline, and 4-hydroxyproline residues and displays similar biomechanical properties to collagen [44]. Alginate is a natural polymer obtained from brown seaweed consisting of β-(1-4) linked to mannouronic acid and β-(1-4) linked with I-glucuronic acid units. It lacks a cell attachment site and is often used with GEL to fabricate 3D scaffolds [45]. Alginate lacks binding properties with GEL; therefore, it was modified to alginate dialdehyde (ADA), offering reactive groups for crosslinking GEL by Schiff base formation [46].

The second step was printing, in which the oscillator shear tests and optimization of bioprinting parameters were performed with the hydrogels. The amplitude sweep analysis is the first step in characterizing the linear viscoelastic region (LVE) of the hydrogels [47].

The LVE region of all the synthesized hydrogels falls within 20 % of the strain, as shown in Fig. 9 A–C. Therefore, further analysis was performed at 1 % strain. The frequency sweep analysis was performed to analyze the storage moduli (G') and loss moduli (G") of the hydrogels, as shown in Fig. 9 D–F.

The formulated hydrogels of ADA-GEL and ACP reinforced ADA-GEL have G' > G", favorable for bioprinting of scaffold. The G' and G" value of hydrogels was analyzed at the lowest frequency of 1 Hz. In the ADA-GEL hydrogel, the G' and G" were 99.2 ± 9.3 Pa and 9 ± 1.1 Pa, respectively. By the addition of ACP_ACE in ADA-GEL hydrogel, the G' and G" of 134.9 ± 16.5 Pa and 6.5 ± 0.5 Pa; on the other hand, incorporation of ACP_CIT in ADA-GEL hydrogel shows G' and G" of 142.6 ± 14.1 Pa and 7.6 ± 1.2 Pa, respectively. The flow behavior of all the formulated hydrogels has non-Newtonian shear thinning properties, as shown in Fig. 9 G.

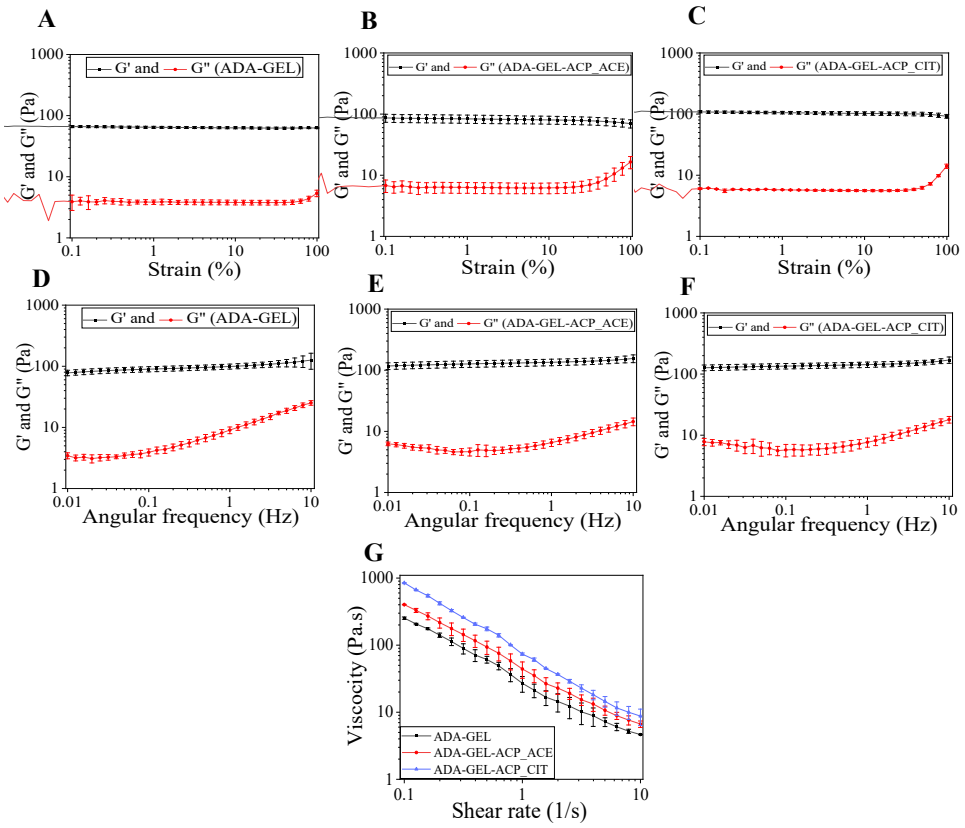

Fig. 9. Oscillatory shear tests of the ADA-GEL and ACP-reinforced ADA-GEL hydrogels. A–C – Amplitude sweep analysis was performed to assess the LVE region of the hydrogel. D–F – Frequency sweep analysis to examine (G') and loss moduli (G") of the hydrogels. Results indicate that reinforcement of ACP in ADA-GEL enhances both G' and loss moduli G" of the ADA-GEL hydrogel. G – A flow behavior analysis of hydrogels was performed using viscosity analysis against shear rate. An increase in the shear rate led to decreased viscosity, revealing the shear-thinning properties of hydrogels.

Further, the printing parameters were optimized by a trial-and-error method using ADA-GEL hydrogel. An 8 × 8 mm^2 construct optimized pressure and printing speed. Initially, the printing was performed slowly at 2 mm/s, and the pressure was varied. Printing speed was adjusted once the construct with the unbroken grid line and uniform pores were obtained, as shown in Fig. 10.

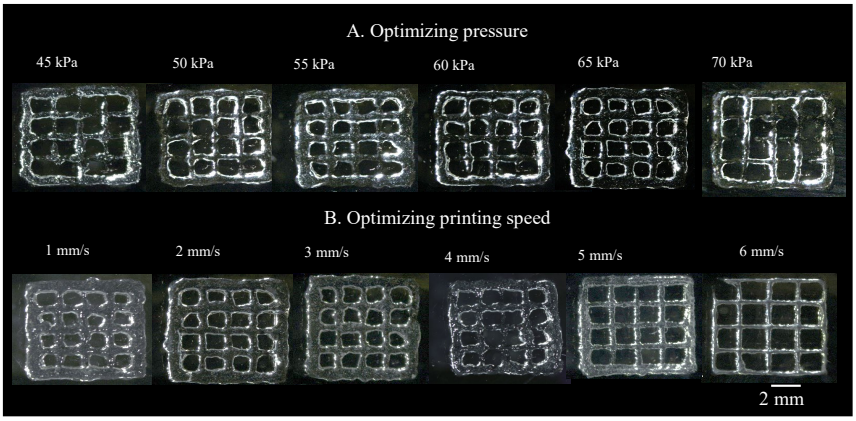

Fig. 10. Trial-and-error approach for evaluating the optimum printing under different printing pressure and speed combinations. A – Initially, the printing pressure was assessed at a slow printing speed of 2 mm/s. B – To overcome this, printing was performed at different speeds, keeping the pressure at 65 kPa.

The optimized printing pressure and speed of 65 kPa and 5 mm/s were used to fabricate constructs with ADA-GEL and ACP-reinforced ADA-GEL bioink, which were further crosslinked (using calcium chloride and microbial transglutaminase) and immersed in α-MEM cell culture media. The third step of post-printing analysis of the construct is essential to ensure the stability of the printed construct. Printability index and average pore area analysis were performed using ImageJ software. The printability index reveals the scaffold's pore geometry, which was analyzed at different day points. Moreover, the results from the printability index were correlated with the average pore area, as shown in Fig. 11.

The pore geometry of the printed constructs was evaluated using the printability index [48]. The circularity (C) of an enclosed area is defined as follows:

$$C = \frac{4\pi A}{L^2}, \tag{1}$$

where L is the perimeter, and A is the area of the pore. Circles have the highest circularity where C equals 1, whereas, for the square shape, circularity equals π/4. Therefore, previous studies have defined the bioink printability index (Pr) based on a square shape using the following function [49]:

$$Pr = \frac{\pi}{4}.\frac{1}{C} = \frac{L^2}{16A}. \tag{2}$$

For an ideal gelation condition, the interconnected channels of the constructs would display a square shape with a *Pr* value of 1. The *Pr* > 1 shows irregular pore geometry, while *Pr* < 1 signifies curved geometry [50]. Optical images of ADA-GEL and ACP-reinforced ADA-GEL constructs were obtained using a stereo microscope. The circularity of pores (n = 16) of each construct was analyzed using ImageJ software (National Institute of Health, Maryland, USA), and *Pr* values were calculated [51]. The data are presented as averages of *Pr* values with standard deviation.

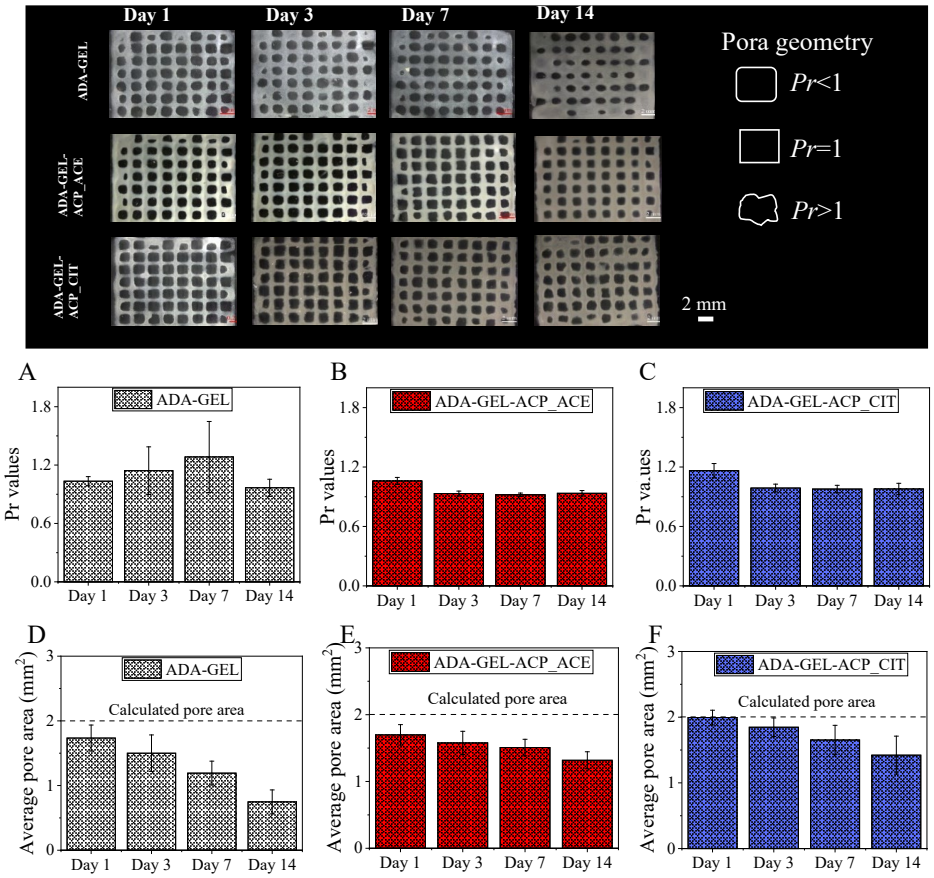

Fig. 11. Post-printing analysis of the printed construct of ADA-GEL and ACP reinforced ADA-GEL bioink (ADA-GEL-ACP_ACE and ADA-GEL-ACP_CIT). Stereo microscopy image analysis was performed on days 1, 3, 7, and 14 (scale bar 2 mm). Printability index (*Pr*) and average pore area analysis were performed using image J analysis by selecting 16 pores. Pore geometry was evaluated by analyzing the *Pr* value; for instance, *Pr* < 1 represents curved, *Pr* = 1 corresponds to square, and *Pr* > 1 resembles variable pore geometry. A–C reveal the *Pr* values. D–F show the average pore area of bioink. ADA-GEL bioinks show rapid conformational changes in pore geometry and reduction in the average pore area of bioink, showing poor structural stability compared to ACP-reinforced ADA-GEL bioinks.

ACP_CIT offers better structural integrity than ACP_ACE, possibly due to the ion release kinetics shown in Fig. 12. The ion release was studied for 168 h (seven days) to analyze calcium and phosphate ion release. Initially, a burst release was observed within the first few hours, gradually reducing over

time [52], [53]. The highest ion release was observed in ACP_CIT, while the calcium and phosphate ions released in ACP_ACE were low, ranging between 1–1.5 mM.

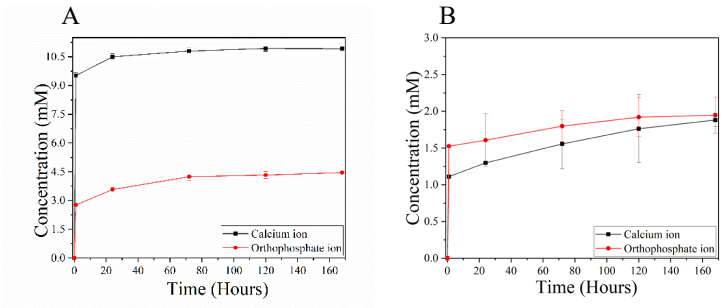

Fig. 12. Kinetic release of phosphate and calcium ions. A) – ACP_CIT and B) – ACP_ACE.

The particle size can also play a crucial role in keeping the structural integrity of the constructs. ACP_ACE has a smaller particle size (~ 20 nm) than ACP_CIT (~ 40 nm) ***(for more details, see Publication 4).*** Smaller particle size provides higher surface area and a higher agglomeration tendency, thus affecting the structural integrity [54].

The carboxylate group of citrates can potentially react with the amine group of gelatins to form amide bond formation. ADA, GEL, or both can be crosslinked with ACP_CIT [55]. However, more advanced analyses are needed to confirm the exact mechanism.

In vitro analysis was performed using Rhodamine phalloidin and DAPI staining. Figure 13 shows cellular attachment on day 1, followed by cell elongation, fusion, and network formation on the consecutive day points. The scaffold surface was covered with cells on day 14, confirming the cytocompatibility of the developed nanocomposite bioink.

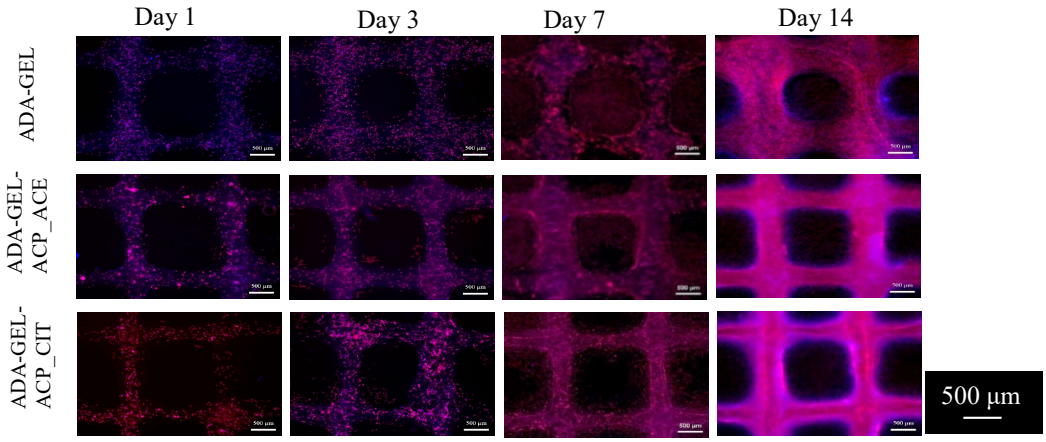

Fig. 13. Epifluorescence microscopy of rhodamine-phalloidin (red) and DAPI (blue) staining of MC3T3-E1 cells embedded in ADA-GEL and ACP reinforced ADA-GEL constructs (ADA-GEL-ACP_ACE and ADA-GEL-ACP_ACE). (Scale bar 500µm).

Two-photon microscopy analyzed the three-dimensional cell distribution within the biofabricated constructs. The 3D reconstructions of the obtained two-photon microscopy image stacks are presented in Fig. 14, showing cell distribution in the scaffolds. The images show that the cell population gradually grows over time in the scaffolds, supporting the results from the epifluorescence microscopy experiments.

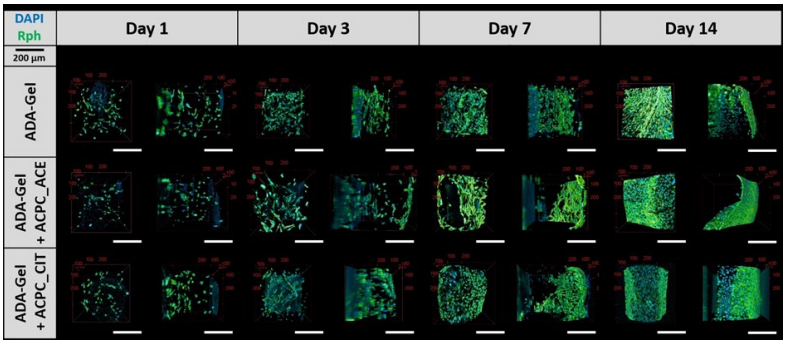

Fig. 14. Three-dimensionally reconstructed multiphoton microscopy images for qualitative morphometry and cell distribution analysis.

NANOCOMPOSITE HYDROGELS

In ***Publication 7***, a nanocomposite hydrogel was developed by incorporating ACP_CIT in the gelatin methacrylate (GELMA) matrix. GELMA is an attractive material in tissue engineering due to its biocompatibility, biodegradability, bioactivity, and unique crosslinking properties in developing nanocomposite hydrogels [56].

A commonly used method for crosslinking GELMA hydrogels is photo-crosslinking, wherein ultraviolet (UV) light and a photo-initiator are used. The GELMA solution has a photo-initiator that is exposed to UV light. The photo-initiator absorbs the UV light and undergoes a photolysis reaction, generating free radicals. The generated free radicals then react with the methacryloyl groups present in GELMA, causing the formation of radicals on the GELMA molecules. The radicals on neighboring GELMA chains start a chain reaction, forming covalent bonds between the methacryloyl groups. Similarly, a redox system uses a chemical initiator, APS and TEMED.

Photo-crosslinking has disadvantages, such as slow in situ gelation and complex preparation processes [57]. One of the significant limitations of photo-crosslinking is the incorporation of fillers that make the hydrogel opaque, which deteriorates light penetration, thus obstructing the photopolymerization reaction process and curing depth [58]. ACP fillers create opaque hydrogel, as shown in Fig. 15 B), which makes photo-crosslinking of GELMA difficult. Therefore, we have utilized the redox initiator chemical crosslinking approach using APS/TEMED to develop GELMA- ACP_CIT hydrogels [59]. The fabricated hydrogels are shown in Fig. 15. Adding ACP_CIT has enhances the viscoelastic properties of GELMA hydrogel.

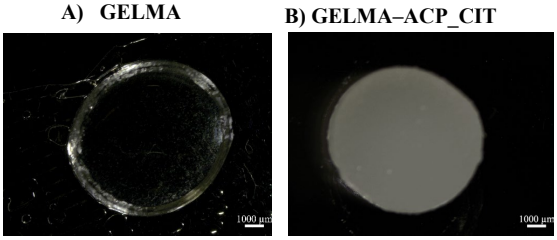

Fig. 15. Fabricated GELMA and GELMA-ACP_CIT hydrogels.

The amplitude sweep is shown in Fig. 16 A–C. The LVE region of the hydrogel was analyzed using amplitude sweep, which falls under 10 % of the stain. Therefore, further analysis was performed under 1 % strain. The storage (G") and loss modulus (G') of the uncrosslinked GELMA was very low (less than 0.1 Pa) with a crossover point (G" = G') of 501 %, indicating its ability to withstand strain-induced irreversible deformation. After cross-linking, the G" and G' of the GELMA hydrogel were enhanced, whereas the crossover point decreased to 125.8 %. Adding ACP-CIT to GELMA hydrogel enhanced the modulus by increasing the crossover point to 158.4 %. The crossover point was enhanced, resulting in hydrogel's ability to withstand strain-induced irreversible deformation.

A frequency sweep analysis was performed to evaluate the viscoelastic properties of the prepared hydrogels, as shown in Fig. 16 D–F. The G' and G" of the hydrogels were analyzed against the frequency of 1 Hz shown in Fig. 16 A. Uncrosslinked GELMA possesses very low G' (0.12 Pa) and G" (0.016 Pa) corresponding to the characteristic of weak and soft material. On the contrary, after crosslinking, the GELMA hydrogel G' (82.6 ± 13 Pa) and G" (2.28 ± 0.5 Pa) were enhanced, corresponding to the increase in strength. Incorporating ACP_CIT have shown further enhancement of G' (318.8 ± 6.5 Pa) and G" (11.3 ± 0.23 Pa) values, conforming reinforcement of GELMA hydrogel.

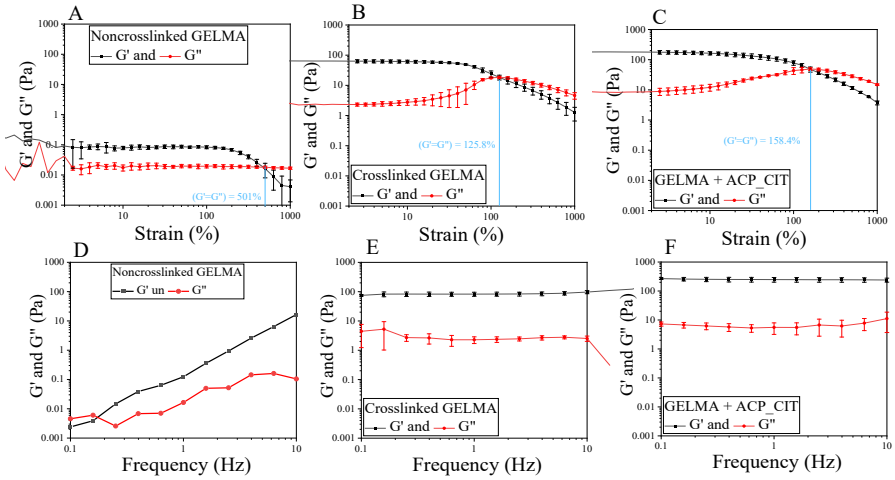

Fig. 16. The viscoelastic properties of the hydrogels were analyzed using oscillatory shear tests: A–C – the LVE region of the hydrogel was analyzed by amplitude sweep; D–F – investigation of storage and loss modulus of the hydrogels by frequency sweep analysis.

The *in vitro* analysis of the developed SN hydrogels was evaluated using rhodamine phalloidin and DAPI staining, as shown in Fig. 17. Cell attachment to the hydrogels was observed on day 1. By day

7, the cells were spread and distributed well on the hydrogel, confirming the cytocompatibility of APS/TEMED crosslinking. Furthermore, ACP_CIT did not harm the proliferation of MC3T3-E1cells.

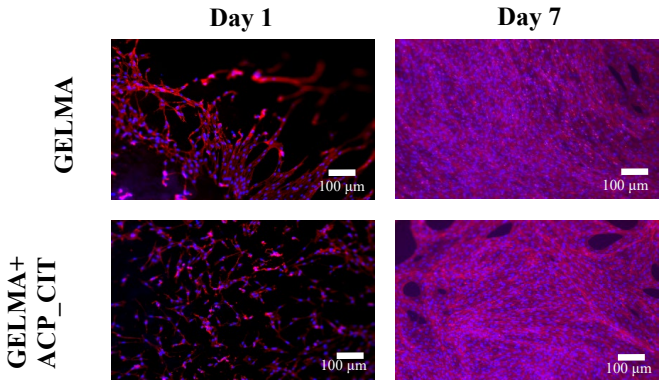

Fig. 17. Fluorescent microscopy of rhodamine-phalloidin (red) and DAPI (blue) staining of MC3T3-E1 cells in GELMA and GELMA-ACP_CIT hydrogels.

NANOCOMPOSITE DOUBLE NETWORK HYDROGELS

In ***Publication 8***, a nanocomposite DN hydrogel consisting of ACP_CIT in a P123-PAM-GELMA matrix was fabricated. The first network of DN hydrogel was created using Pluronic P123. The second network consists of polyacrylamide (PAM) and GELMA co-polymers. The second network was crosslinked using ammonium persulfate (APS) and N,N,N′,N′-Tetramethylethylenediamine (TEMED), as shown in Fig. 18.

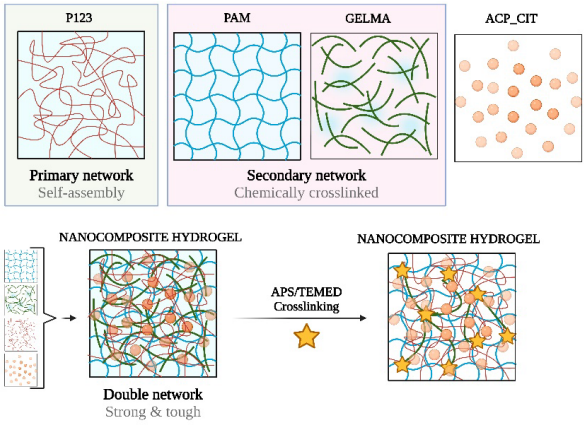

Fig. 18. Development of DN hydrogel by a physical-chemical network. Pluronic P123 self-assembly was used as a primary network, and the secondary network was composed of a co-polymer system made up of polyacrylamide-gelatin methacrylate (PAM-GELMA). Moreover, the ACP_CIT was utilized as an inorganic filler.

A systematic approach was deployed for preparation for DN nanocomposite hydrogels; initially, the impact of varying w/v concentration of P123 (2.5 %, 5 %, 7.5 %, and 10 %) on mechanical

properties (Young's modulus, tensile strength, elongation at break) of PAM-GELMA was explored. Amongst these, the DN hydrogel with 7.5 w/v% P123 in PAM-GELMA (DN3) exhibited the highest mechanical properties; therefore, it was further used for the development of nanocomposite DN hydrogels by incorporating different w/v concentrations of ACP_CIT (0.75 %, 1.5 %, and 3 %) in P123.

The nanocomposite DN hydrogels with 0.75 % w/v ACP_CIT (abbreviated as DN3-ACP0.75) exhibited the highest mechanical properties (as shown in Fig. 19), whose rheological characteristics and cytocompatibility were further evaluated and compared with pristine DN hydrogel (7.5 w/v% P123-PAM-GELMA) (abbreviated as DN3).

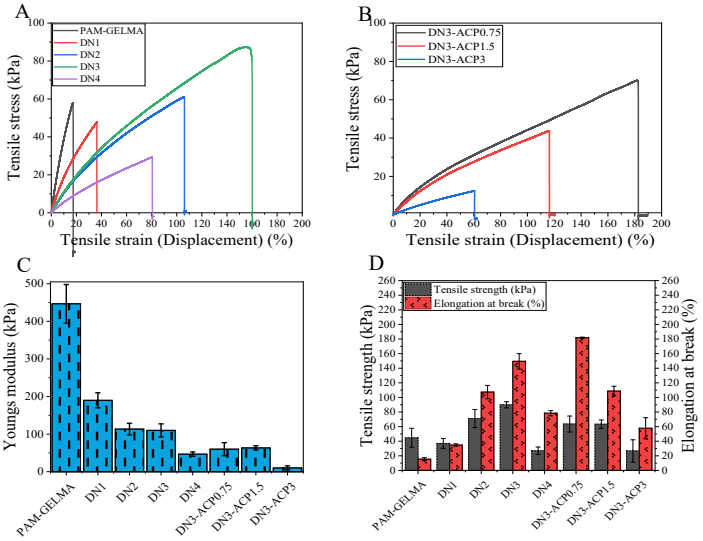

Fig. 19. Tensile stress-strain curve of the prepared hydrogel. A – Analyzing the effect of P123 concentration on the Elongation of the PAM-GELMA hydrogel; B – analyzing the effect of ACP_CIT concentration on the Elongation of the DN3 hydrogel; C – Young's modulus; D – tensile strength, and elongation at break (%) of all the synthesized hydrogels.

The amplitude sweep of all the synthesized hydrogels reveals that the hydrogels possess G' > G", showing gel-like behavior. A frequency sweep analysis was performed to evaluate the viscoelastic properties of the prepared hydrogels ***(for more details, see Publication 8)***. The G' and G" of the hydrogels were analyzed against the frequency of 1 Hz shown in Fig. 20 A. P123 possesses very low G' (1904 ± 50 Pa) and G" (1112.3 ± 28.5 Pa), corresponding to the characteristic of weak and soft material. On the contrary, the PAM-GELMA hydrogel has high G' (10916.6 ± 625.3 Pa) and G" (4058.6 ± 213.8 Pa), corresponding to the high strength and brittle nature. By increasing the P123 in PAM-GELMA hydrogel, the G' value was less affected compared to the G" value. The reduction in G" means less energy is dissipated during deformation, indicating that the hydrogel behaves more elastically and less viscously. Therefore, as the concentration of P123 increases, the difference between the G' and G" values shows increasing elastic behavior [60]. This phenomenon was observed until the P123 concentration of 7.5 w/v% in PAM-GELMA hydrogel (DN3). However, further increasing the P123 concentration to 10 w/v% in PAM-GELMA hydrogel (DN4), the decrease in the G' and increase in G", obstructed the elastic behavior of the hydrogel.

In the case of nanocomposite hydrogels at lower concentration of ACP_CIT (0.75 % w/v) in DN3 hydrogels (DN3-ACP0.75), reveals the G' of 9141 ± 2545 Pa and G" of 341.3 ± 134.8 Pa. The incorporation of ACP_CIT (0.75 % w/v) decreases G' and G" values, however the reduction in the G' was marginal while G" values drastically decreased, which may be responsible for enhancing elastic property. However, as the concentration of ACP_CIT (1.5 % w/v) increased in DN3 hydrogels (DN3-ACP1.5) drastically increased values of G' (17766.6 ± 2689.4 Pa) and G" of (1034.9 ± 290.2 Pa) imparting rigidity to the hydrogel. A further increase in ACP_CIT concentration (3 % w/v) in DN3 hydrogels (DN3-ACP3) shows extreme enhancement on G' (22523.3 ± 6950 Pa) and G" of (1422.6 ± 47.6 Pa), which may be responsible for compromising the mechanical properties [61], [62].

The tan δ analysis of all the synthesized hydrogels is shown in Fig. 20 C. Tan δ is the ratio of G" to G' of viscoelastic material often used to analyze the damping properties of the material. It quantifies the ratio of energy dissipated as heat. In viscoelastic material, a higher tan δ value (close to 1) indicates a higher proportion of energies dissipated as heat relative to the energy stored elastically. On the other hand, a lower tan δ value indicates that more energy is elastically stored compared to dissipated energy [47].

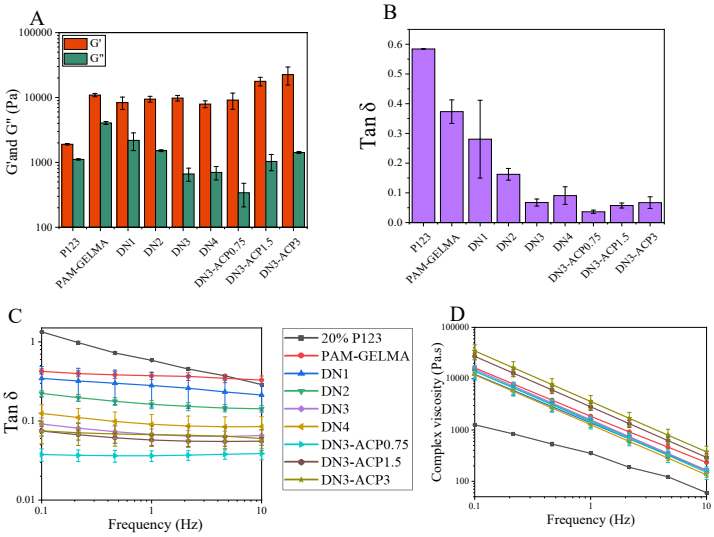

Fig. 20. A – Analyzing storage (G') loss modulus (G") at the frequency of 1 Hz. B –Evaluation of the tan δ at 1 Hz. C – Tan δ analyzed all synthesized hydrogels at varying frequencies. D – Complex viscosity.

The tan δ of PAM-GELMA hydrogel was 0.37±0.03 when analyzed at a frequency of 1 Hz, shown in Fig. 20 D. Increasing P123 concentration in PAM-GELMA hydrogels shows tan δ of 0.28±0.13 (DN1), 0.16 ± 0.01 (DN2), 0.067 ± 0.01 (DN3) and 0.09 ± 0.02 (DN4), respectively. This analysis revealed that tan δ values decreased till the P123 concentration was 7.5 % w/v in PAM-GELMA (DN3), which can be attributed to increased flexibility [63]. However, when the P123 concentration was increased to 10 % w/v in PAM-GELMA (DN4), the tan δ value increased, thus hindering the damping properties and reducing flexibility.

In the nanocomposite hydrogels, the tan δ values were 0.036 ± 0.05 (DN3-ACP0.75), 0.057 ± 0.008 (DN3-ACP1.5), and 0.067 ± 0.02 (DN3-ACP3). The tan δ value of DN3-ACP0.75 was

the lowest, which can be attributed to the highest elasticity. Increasing the concentration of ACP_CIT in DN3 hydrogels to 1.5 % w/v (DN3-ACP1.5) and 3 % w/v (DN3-ACP3) increases the tan δ value, which can be attributed to the reduction in the damping properties. With the increase in the ACP_CIT concentration, the tan δ value starts to increase, which can alter the crosslinking density and polymer chain mobility within the hydrogel, thus affecting the hydrogel's overall mechanical properties.

The complex viscosity of all the synthesized hydrogel decreased with an increase in frequency, demonstrating shear thinning behavior. Variations in the complex viscosities were observed with different concentrations of P123 and ACP_CIT in PAM-GELMA hydrogel [64]. As shown in Fig. 20 D, an increase in P123 concentration in PAM-GELMA hydrogel led to a notable reduction in complex viscosity.

The results from tensile strength analysis go hand in hand with the oscillatory shear tests, confirming that blending of P123 enhances the elasticity and mechanical properties of PAM-GELMA hydrogels. However, the performance of P123 was concentration-dependent. In addition, the performance of ACP_CIT was also concentration-dependent. At deficient concentrations, enhancement in elasticity was observed, which may be due to pseudo crosslinking of citrate in ACP_CIT with GELMA. However, more advanced analyses are required to confirm the ACP_CIT-GELMA interaction. The DN3 and its nanocomposite DN3-ACP0.75 hydrogel have the highest mechanical properties. Therefore, further analysis was performed on these two hydrogels.

Creep and recovery behavior help reflect the interaction of polymeric chains of the viscoelastic material, which helps to understand and analyze the deformation mechanism of the hydrogels. Therefore, the creep recovery analysis was performed to evaluate the interaction change among the polymer chain of the one DN3 and nanocomposite DN3-ACP0.75 hydrogels, as shown in Fig. 21 A. The incorporation of ACP_CIT in DN3 hydrogel (DN3-ACP0.75) shows a positive effect on decreasing creep strain. This can be due to restricted polymer chain movements by adding ACP_CIT nanoparticles [65]. The stress relaxation curves are presented in Fig. 21 B. The DN3 and nanocomposite DN3-ACP0.75 hydrogels show rapid stress relaxations.

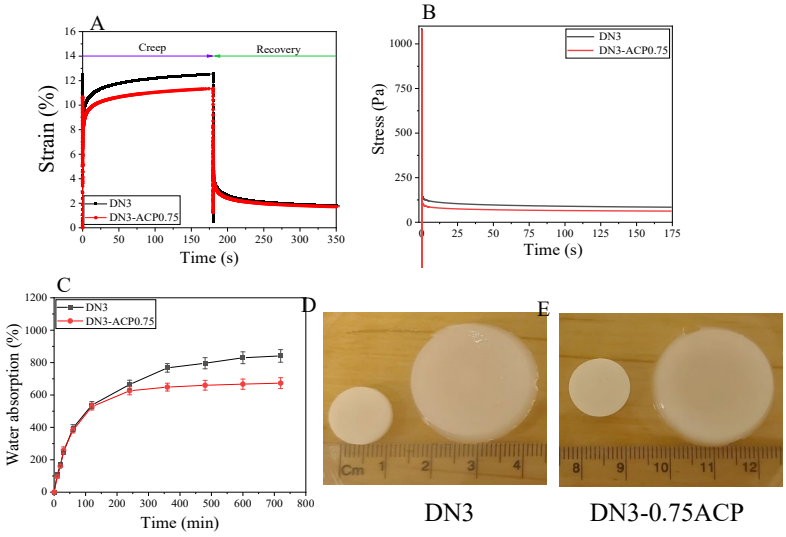

Fig. 21. Analyzing creep-recovery (A), stress relaxation (B), water uptake capacity (C), and photographs of dried and swelled DN3 and DN3-ACP0.75 hydrogels (D and E).

The water uptake capacity of DN3 hydrogel and its composite DN3-ACP0.75 is presented in Fig. 21 C. Both the DN3 and DN3-ACP0.75 hydrogels grow double in size after swelling, as observed in Fig. 21 D and E. The incorporation of ACP_CIT in the DN3 hydrogel affects the swelling kinetics. A reduction in the water uptake capacity of DN3-ACP0.75 hydrogels can be due to the hindrance of the free polymer chain movement by the addition of ACP_CIT [66].

The shape memory hydrogel possesses two different types of crosslinks. One of the crosslinks is composed of a covalent network, which is essential to maintaining the structural integrity of the hydrogel. On the other hand, the second crosslink is composed of a physical reversible network responsible for fixing the temporary shape. In this investigation, PAM-GELMA forms the covalently crosslinked network [67]. The thermosensitive P123 forms reverse physical crosslinking when exposed to high temperature (70 ℃), triggering the temporary shape formation when exposed to (4 ℃), thus providing shape memory and recovery properties, as shown in Fig. 22.

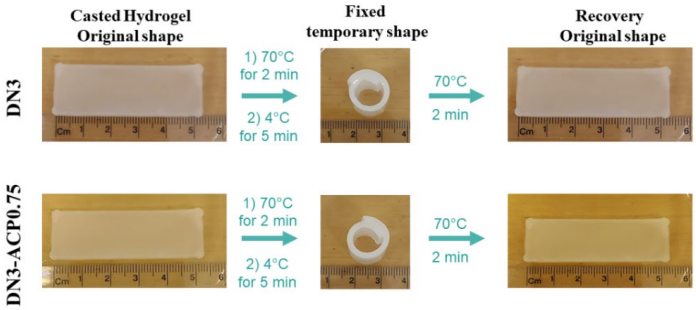

Fig. 22. Temperature-induced shape memory behavior of DN3 and DN3-ACP0.75 hydrogels.

In vitro analysis of the fabricated hydrogel was evaluated using rhodamine phalloidin and DAPI staining, as shown in Fig. 23. The cell attachment on the hydrogel was observed on day 1. On day 3, the cells spread well and were distributed on both hydrogels. On day 7, the scaffold was densely populated with cells, confirming the cytocompatibility of developed DN3 and DN3-ACP0.75 hydrogels.

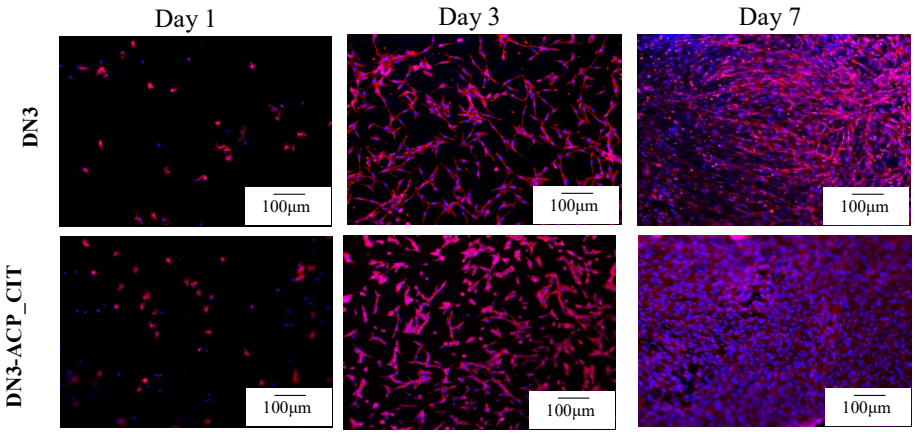

Fig. 23. Fluorescent microscopy of rhodamine-phalloidin (red) and DAPI (blue) staining of MC3T3-E1 cells in DN3 and DN3-ACP0.75 hydrogels.

CONCLUSIONS

1. The variation in the negative charge within the side chain of SOMs influences the interaction of SOMs with ACP, consequently impacting the physiological properties of ACP.
2. Solution-mediated transformation kinetics of ACP to Ap is affected by the media composition. However, the transformation order remains consistent across different media compositions: ACP_ACE>>pure ACP=ACP_ITN=ACP_GLU>>ACP_ASC>>ACP_CIT. In PBS, all the synthesized ACPs showed accelerated transformation to Ap compared to DI water. The presence of phosphate ions in PBS reduces the ACP stability, thus accelerating Ap formation. α-MEM shows slower transformation kinetics than PBS, attributed to its lower concentration of phosphate ions.
3. The addition of 1 % w/v ACP_CIT and ACP_ACE to ADA-GEL hydrogel increases both the storage and loss modulus (G' = 142.6 ± 14.1 Pa and G" = 7.6 ± 1.2 Pa for ACP_CIT, G' = 134.9 ± 16.5 Pa and G" = 6.5 ± 0.5 Pa for ACP_ACE, and G' = 99.2 ± 9.3 Pa and G" = 9 ± 1.1 Pa for ADA-GEL hydrogel). Enhancements in the storage and loss modulus improved the printed scaffold's structural integrity. The enhancement can be attributed to the additional calcium ions provided by ACP for ADA crosslinking.
4. The GELMA hydrogel possesses G' (82.6 ± 13 Pa) and G" (2.28 ± 0.5 Pa) addition of 2 % w/v ACP_CIT to GELMA hydrogel enhanced G' (318.8 ± 6.5 Pa) and G" (11.3 ± 0.23 Pa) values, thus confirming reinforcement of GELMA hydrogel by addition of ACP_CIT.
5. The effect of ACP_CIT on the mechanical properties of DN3 hydrogel was concentration-dependent. Adding 0.75 % w/v ACP_CIT increases the flexibility of DN3 hydrogel, which can be attributed to the reduction in polymer chain entanglement by the small amount of ACP_CIT. However, as the concentration of ACP_CIT increased, the G' and G" values drastically increased, thus imparting rigidity to the hydrogel, resulting in compromised mechanical properties.

REFERENCES

[1] J. M. Grasman, M. J. Zayas, R. L. Page, and G. D. Pins, "Biomimetic Scaffolds for Regeneration of Volumetric Muscle Loss in Skeletal Muscle Injuries," *Acta Biomater.*, vol. 25, p. 2, Oct. 2015, doi: 10.1016/J.ACTBIO.2015.07.038.

[2] "Musculoskeletal health." Accessed: Dec. 13, 2023. [Online]. Available: https://www.who.int/news-room/fact-sheets/detail/musculoskeletal-conditions

[3] A. R. Amini, C. T. Laurencin, and S. P. Nukavarapu, "Bone Tissue Engineering: Recent Advances and Challenges," *Crit. Rev. Biomed. Eng.*, vol. 40, no. 5, p. 363, 2012, doi: 10.1615/CRITREVBIOMEDENG.V40.I5.10.

[4] A. H. Schmidt, "Autologous bone graft: Is it still the gold standard?," *Injury*, vol. 52, pp. S18–S22, Jun. 2021, doi: 10.1016/J.INJURY.2021.01.043.

[5] O. Petrauskaite *et al.*, "Biomimetic mineralization on a macroporous cellulose-based matrix for bone regeneration," *Biomed Res. Int.*, vol. 2013, 2013, doi: 10.1155/2013/452750.

[6] A. L. Lehninger, "Mitochondria and Calcium Ion Transport THE FIFTH JUBILEE LECTURE," *Biochem. J.*, vol. 119, no. 2, pp. 129–138, 1970.

[7] J. H. Bradt, M. Mertig, A. Teresiak, and W. Pompe, "Biomimetic Mineralization of Collagen by Combined Fibril Assembly and Calcium Phosphate Formation," *Chem. Mater.*, vol. 11, no. 10, pp. 2694–2701, 1999, doi: 10.1021/CM991002P.

[8] A. G. Walton, B. A. Friedman, and A. Schwartz, "Nucleation and mineralization of organic matrices," *J. Biomed. Mater. Res.*, vol. 1, no. 3, pp. 337–354, Sep. 1967, doi: 10.1002/JBM.820010305.

[9] "Biomedical Applications of Inorganic Materials," *Biomed. Appl. Inorg. Mater.*, Dec. 2021, doi: 10.1039/9781788019293.

[10] C. Drouet, "Apatite formation: Why it may not work as planned, and how to conclusively identify apatite compounds," *Biomed Res. Int.*, vol. 2013, 2013, doi: 10.1155/2013/490946.

[11] A. Indurkar, R. Choudhary, K. Rubenis, and J. Locs, "Advances in Sintering Techniques for Calcium Phosphates Ceramics," *Mater. 2021, Vol. 14, Page 6133*, vol. 14, no. 20, p. 6133, Oct. 2021, doi: 10.3390/MA14206133.

[12] H. C. W. Skinner and H. Ehrlich, "Biomineralization," *Treatise Geochemistry Second Ed.*, vol. 10, pp. 105–162, Jan. 2014, doi: 10.1016/B978-0-08-095975-7.00804-4.

[13] I. Cacciotti, "Cationic and anionic substitutions in hydroxyapatite," *Handb. Bioceram. Biocomposites*, pp. 145–211, Jan. 2016, doi: 10.1007/978-3-319-12460-5_7/FIGURES/6.

[14] A. Lotsari, A. K. Rajasekharan, M. Halvarsson, and M. Andersson, "Transformation of amorphous calcium phosphate to bone-like apatite," *Nat. Commun. 2018 91*, vol. 9, no. 1, pp. 1–11, Oct. 2018, doi: 10.1038/s41467-018-06570-x.

[15] A. Indurkar, R. Choudhary, K. Rubenis, and J. Locs, "Role of carboxylic organic molecules in interfibrillar collagen mineralization," *Front. Bioeng. Biotechnol.*, vol. 11, p. 439, Apr. 2023, doi: 10.3389/FBIOE.2023.1150037.

[16] W. J. Landis, F. H. Silver, and J. W. Freeman, "Collagen as a scaffold for biomimetic mineralization of vertebrate tissues," *J. Mater. Chem.*, vol. 16, no. 16, pp. 1495–1503, 2006, doi: 10.1039/B505706J.

[17] W. J. Landis and F. H. Silver, "Mineral Deposition in the Extracellular Matrices of Vertebrate Tissues: Identification of Possible Apatite Nucleation Sites on Type I Collagen," *Cells. Tissues. Organs*, vol. 189, no. 1–4, p. 20, Dec. 2008, doi: 10.1159/000151454.

[18] Y. K. Kim *et al.*, "Mineralisation of reconstituted collagen using polyvinylphosphonic acid/polyacrylic acid templating matrix protein analogues in the presence of calcium, phosphate and hydroxyl ions," *Biomaterials*, vol. 31, no. 25, p. 6618, Sep. 2010, doi: 10.1016/J.BIOMATERIALS.2010.04.060.

[19] A. Pouikli *et al.*, "Chromatin remodeling due to degradation of citrate carrier impairs osteogenesis of aged mesenchymal stem cells," *Nat. Aging 2021 19*, vol. 1, no. 9, pp. 810–825, Sep. 2021, doi: 10.1038/s43587-021-00105-8.

[20] Y. Wang *et al.*, "Aging Relevant Metabolite Itaconate Inhibits Inflammatory Bone Loss," *Front.*

Endocrinol. (Lausanne)., vol. 13, Jul. 2022, doi: 10.3389/FENDO.2022.885879/FULL.
[21] K. S. Brakspear and D. J. Mason, "Glutamate signaling in bone," *Front. Endocrinol. (Lausanne).*, vol. 3, no. AUG, 2012, doi: 10.3389/FENDO.2012.00097.
[22] O. Polat, S. S. Kilicoglu, and E. Erdemli, "A controlled trial of glutamine effects on bone healing," *Adv. Ther.*, vol. 24, no. 1, pp. 154–160, May 2007, doi: 10.1007/BF02850003.
[23] F. Dickens, "The citric acid content of animal tissues, with reference to its occurrence in bone and tumour," *Biochem. J.*, vol. 35, no. 8–9, pp. 1011–1023, Sep. 1941, doi: 10.1042/BJ0351011.
[24] D. Granchi, N. Baldini, F. M. Ulivieri, and R. Caudarella, "Role of Citrate in Pathophysiology and Medical Management of Bone Diseases," *Nutrients*, vol. 11, no. 11, 2019, doi: 10.3390/NU11112576.
[25] E. Davies *et al.*, "Citrate bridges between mineral platelets in bone," *Proc. Natl. Acad. Sci. U. S. A.*, vol. 111, no. 14, 2014, doi: 10.1073/PNAS.1315080111/-/DCSUPPLEMENTAL/PNAS.201315080SI.PDF.
[26] B. Xie and G. H. Nancollas, "How to control the size and morphology of apatite nanocrystals in bone," *Proc. Natl. Acad. Sci. U. S. A.*, vol. 107, no. 52, p. 22369, Dec. 2010, doi: 10.1073/PNAS.1017493108.
[27] S. Murad, D. Grove, K. A. Lindberg, G. Reynolds, A. Sivarajah, and S. R. Pinnell, "Regulation of collagen synthesis by ascorbic acid.," *Proc. Natl. Acad. Sci. U. S. A.*, vol. 78, no. 5, p. 2879, 1981, doi: 10.1073/PNAS.78.5.2879.
[28] D. Gunson, K. E. Gropp, and A. Varela, "Bone and Joints," *Haschek Rousseaux's Handb. Toxicol. Pathol. Third Ed. Vol. 1-3*, vol. 1–3, pp. 2761–2858, Jan. 2013, doi: 10.1016/B978-0-12-415759-0.00063-7.
[29] R. Thaler *et al.*, "Vitamin C epigenetically controls osteogenesis and bone mineralization," *Nat. Commun. 2022 131*, vol. 13, no. 1, pp. 1–18, Oct. 2022, doi: 10.1038/s41467-022-32915-8.
[30] P. Aghajanian, S. Hall, M. D. Wongworawat, and S. Mohan, "The Roles and Mechanisms of Actions of Vitamin C in Bone: New Developments," *J. Bone Miner. Res.*, vol. 30, no. 11, p. 1945, Nov. 2015, doi: 10.1002/JBMR.2709.
[31] C. Combes and C. Rey, "Amorphous calcium phosphates: synthesis, properties and uses in biomaterials," *Acta Biomater.*, vol. 6, no. 9, pp. 3362–3378, 2010, doi: 10.1016/J.ACTBIO.2010.02.017.
[32] A. L. Boskey and A. S. Posner, "Conversion of amorphous calcium phosphate to microcrystalline hydroxyapatite. A pH-dependent, solution-mediated, solid-solid conversion," *J. Phys. Chem.*, vol. 77, no. 19, pp. 2313–2317, 1973, doi: 10.1021/J100638A011/SUPPL_FILE/J100638A011_SI_001.PDF.
[33] L. N. Niu *et al.*, "Biomimetic remineralization of dentin," *Dent. Mater.*, vol. 30, no. 1, pp. 77–96, Jan. 2014, doi: 10.1016/J.DENTAL.2013.07.013.
[34] A. J. Hoeher, S. T. Mergelsberg, O. J. Borkiewicz, and F. M. Michel, "Impacts of Initial Ca/P on Amorphous Calcium Phosphate," 2023, doi: 10.1021/acs.cgd.1c00058.
[35] M. Iafisco *et al.*, "Fluoride-doped amorphous calcium phosphate nanoparticles as a promising biomimetic material for dental remineralization," *Sci. Rep.*, vol. 8, no. 1, Dec. 2018, doi: 10.1038/S41598-018-35258-X.
[36] J. M. Ten Cate and J. D. B. Featherstone, "Mechanistic aspects of the interactions between fluoride and dental enamel," *Crit. Rev. Oral Biol. Med.*, vol. 2, no. 3, pp. 283–296, 1991, doi: 10.1177/10454411910020030101.
[37] K. Chatzipanagis *et al.*, "Crystallization of citrate-stabilized amorphous calcium phosphate to nanocrystalline apatite: a surface-mediated transformation," *CrystEngComm*, vol. 18, no. 18, pp. 3170–3173, May 2016, doi: 10.1039/C6CE00521G.
[38] S. Dominguez-Medina, S. McDonough, P. Swanglap, C. F. Landes, and S. Link, "In situ measurement of bovine serum albumin interaction with gold nanospheres," *Langmuir*, vol. 28, no. 24, pp. 9131–9139, Jun. 2012, doi: 10.1021/LA3005213.
[39] G. P. Szekeres and J. Kneipp, "Different binding sites of serum albumins in the protein corona of gold nanoparticles," *Analyst*, vol. 143, no. 24, pp. 6061–6068, Dec. 2018, doi: 10.1039/C8AN01321G.

[40] D. Schubert and D. Piasecki, “Oxidative Glutamate Toxicity Can Be a Component of the Excitotoxicity Cascade,” *J. Neurosci.*, vol. 21, no. 19, p. 7455, Oct. 2001, doi: 10.1523/JNEUROSCI.21-19-07455.2001.

[41] A. A. Kritis, E. G. Stamoula, K. A. Paniskaki, and T. D. Vavilis, “Researching glutamate – induced cytotoxicity in different cell lines: A comparative/collective analysis/study,” *Front. Cell. Neurosci.*, vol. 9, p. 131867, Mar. 2015, doi: 10.3389/FNCEL.2015.00091/BIBTEX.

[42] P. W. Hwang and J. A. Horton, “Variable osteogenic performance of MC3T3-E1 subclones impacts their utility as models of osteoblast biology,” *Sci. Reports 2019 91*, vol. 9, no. 1, pp. 1–9, Jun. 2019, doi: 10.1038/s41598-019-44575-8.

[43] S. N. Hadzir *et al.*, “Ascorbic acid induces osteoblast differentiation of human suspension mononuclear cells,” *Cytotherapy*, vol. 16, no. 5, pp. 674–682, May 2014, doi: 10.1016/J.JCYT.2013.07.013.

[44] T. Fukunishi, T. Shoji, and T. Shinoka, “Nanofiber composites in vascular tissue engineering,” *Nanofiber Compos. Biomed. Appl.*, pp. 455–481, Jan. 2017, doi: 10.1016/B978-0-08-100173-8.00018-1.

[45] M. B. Łabowska, K. Cierluk, A. M. Jankowska, J. Kulbacka, J. Detyna, and I. Michalak, “A Review on the Adaption of Alginate-Gelatin Hydrogels for 3D Cultures and Bioprinting,” *Materials (Basel).*, vol. 14, no. 4, pp. 1–28, Feb. 2021, doi: 10.3390/MA14040858.

[46] S. Heid *et al.*, “Bioprinting with bioactive alginate dialdehyde-gelatin (ADA-GEL) composite bioinks: Time-dependent in-situ crosslinking via addition of calcium-silicate particles tunes in vitro stability of 3D bioprinted constructs,” *Bioprinting*, vol. 26, p. e00200, Jun. 2022, doi: 10.1016/J.BPRINT.2022.E00200.

[47] A. Indurkar, P. Bangde, M. Gore, P. Reddy, R. Jain, and P. Dandekar, “Optimization of guar gum-gelatin bioink for 3D printing of mammalian cells,” *Bioprinting*, vol. 20, p. e00101, Dec. 2020, doi: 10.1016/J.BPRINT.2020.E00101.

[48] H. Jongprasitkul, S. Turunen, V. S. Parihar, and M. Kellomäki, “Two-step crosslinking to enhance the printability of methacrylated gellan gum biomaterial ink for extrusion-based 3D bioprinting,” *Bioprinting*, vol. 25, Mar. 2022, doi: 10.1016/J.BPRINT.2021.E00185.

[49] S. Kyle, Z. M. Jessop, A. Al-Sabah, and I. S. Whitaker, “‘Printability’’ of Candidate Biomaterials for Extrusion Based 3D Printing: State-of-the-Art,’” *Adv. Healthc. Mater.*, vol. 6, no. 16, Aug. 2017, doi: 10.1002/ADHM.201700264.

[50] L. Ouyang, “3D Bioprinting of Thermal-Sensitive Bioink,” pp. 63–80, 2019, doi: 10.1007/978-981-13-9455-3_5.

[51] W. Rasband, “ImageJ, U.S. National Institutes of Health, Bethesda, Maryland, USA,” 2011.

[52] X. Niu, S. Chen, F. Tian, L. Wang, Q. Feng, and Y. Fan, “Hydrolytic conversion of amorphous calcium phosphate into apatite accompanied by sustained calcium and orthophosphate ions release,” *Mater. Sci. Eng. C*, vol. 70, pp. 1120–1124, Jan. 2017, doi: 10.1016/J.MSEC.2016.04.095.

[53] X. Niu *et al.*, “Sustained delivery of calcium and orthophosphate ions from amorphous calcium phosphate and poly(L-lactic acid)-based electrospinning nanofibrous scaffold,” *Sci. Reports 2017 71*, vol. 7, no. 1, pp. 1–9, Mar. 2017, doi: 10.1038/srep45655.

[54] Y. Cai, S. Y. Chang, S. W. Gan, S. Ma, W. F. Lu, and C. C. Yen, “Nanocomposite bioinks for 3D bioprinting,” *Acta Biomater.*, vol. 151, pp. 45–69, Oct. 2022, doi: 10.1016/J.ACTBIO.2022.08.014.

[55] M. Inoue, M. Sasaki, A. Nakasu, M. Takayanagi, and T. Taguchi, “An antithrombogenic citric acid-crosslinked gelatin with endothelialization activity,” *Adv. Healthc. Mater.*, vol. 1, no. 5, pp. 573–581, Sep. 2012, doi: 10.1002/ADHM.201200001.

[56] S. Bupphathong, C. Quiroz, W. Huang, P. F. Chung, H. Y. Tao, and C. H. Lin, “Gelatin Methacrylate Hydrogel for Tissue Engineering Applications—A Review on Material Modifications,” *Pharmaceuticals*, vol. 15, no. 2, Feb. 2022, doi: 10.3390/PH15020171.

[57] J. Zhang *et al.*, “Injectable In Situ Photocrosslinked Hydrogel Dressing for Infected Wound Healing,” *ACS Appl. Bio Mater.*, vol. 6, no. 5, pp. 1992–2002, May 2023, doi: 10.1021/ACSABM.3C00205/SUPPL_FILE/MT3C00205_SI_001.PDF.

[58] Q. Ma, Y. Zhang, V. Launay, M. Le Dot, S. Liu, and J. Lalevée, "How to overcome the light penetration issue in photopolymerization? An example for the preparation of high content iron-containing opaque composites and application in 3D printing," *Eur. Polym. J.*, vol. 165, p. 111011, Feb. 2022, doi: 10.1016/J.EURPOLYMJ.2022.111011.

[59] Y. Stuart, F. Lauren, and A. Brian, "A mechanically robust injectable hydrogel scaffold for adipose-derived stem cell delivery for the treatment of peripheral arterial disease," *Front. Bioeng. Biotechnol.*, vol. 4, 2016, doi: 10.3389/CONF.FBIOE.2016.01.00861/EVENT_ABSTRACT.

[60] H. Chen, S. Hou, H. Ma, X. Li, and Y. Tan, "Controlled gelation kinetics of cucurbit[7]uril-adamantane cross-linked supramolecular hydrogels with competing guest molecules," *Sci. Reports 2016 61*, vol. 6, no. 1, pp. 1–10, Feb. 2016, doi: 10.1038/srep20722.

[61] J. Zaragoza, S. Fukuoka, M. Kraus, J. Thomin, and P. Asuri, "Exploring the Role of Nanoparticles in Enhancing Mechanical Properties of Hydrogel Nanocomposites," *Nanomater. 2018, Vol. 8, Page 882*, vol. 8, no. 11, p. 882, Oct. 2018, doi: 10.3390/NANO8110882.

[62] M. Levin, A. Sonn-Segev, and Y. Roichman, "Structural changes in nanoparticle-hydrogel composites at very low filler concentrations," *J. Chem. Phys.*, vol. 150, no. 6, Feb. 2019, doi: 10.1063/1.5053171/198966.

[63] Z. Jing *et al.*, "Tough, stretchable and compressive alginate-based hydrogels achieved by non-covalent interactions," *RSC Adv.*, vol. 10, no. 40, pp. 23592–23606, Jun. 2020, doi: 10.1039/D0RA03733H.

[64] G. Kaya and F. Oytun, "Rheological properties of İnjectable hyaluronic acid hydrogels for soft tissue engineering applications," *Biointerface Res. Appl. Chem.*, vol. 11, no. 1, pp. 8424–8430, 2021, doi: 10.33263/BRIAC111.84248430.

[65] S. Shojaei, M. Nikuei, V. Goodarzi, M. Hakani, H. A. Khonakdar, and M. R. Saeb, "Disclosing the role of surface and bulk erosion on the viscoelastic behavior of biodegradable poly(ε-caprolactone)/poly(lactic acid)/hydroxyapatite nanocomposites," *J. Appl. Polym. Sci.*, vol. 136, no. 10, p. 47151, Mar. 2019, doi: 10.1002/APP.47151.

[66] B. Y. S. Kumar, A. M. Isloor, G. C. M. Kumar, Inamuddin, and A. M. Asiri, "Nanohydroxyapatite Reinforced Chitosan Composite Hydrogel with Tunable Mechanical and Biological Properties for Cartilage Regeneration," *Sci. Reports 2019 91*, vol. 9, no. 1, pp. 1–13, Nov. 2019, doi: 10.1038/s41598-019-52042-7.

[67] B. Maiti *et al.*, "Thermoresponsive Shape-Memory Hydrogel Actuators Made by Phototriggered Click Chemistry," *Adv. Funct. Mater.*, vol. 30, no. 24, p. 2001683, Jun. 2020, doi: 10.1002/ADFM.202001683.

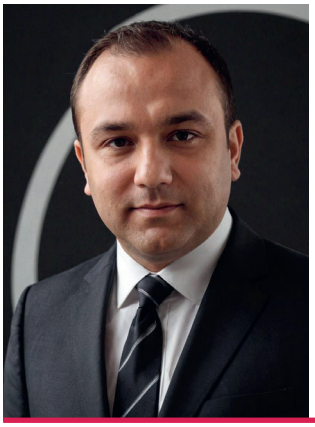

Abhishek Rajesh Indurkar was born in 1994 in Bhusawal, India. He holds a Bachelor's degree in Biotechnology Engineering (2017) and a Master's degree in Pharmaceutical Biotechnology (2019). In 2020, Abhishek began his doctoral studies under the supervision of Professor Jānis Ločs and Senior Researcher Kristaps Rubenis at Riga Technical University and the Baltic Biomaterial Centre of Excellence. During his postgraduate studies, he completed a secondment at Friedrich-Alexander-Universität Erlangen-Nürnberg, Germany, under the guidance of Professor Aldo R. Boccaccini.

His research interests focus on bioprinting, bioink formulations, and nanocomposite development to create artificial tissues and human organs.